Universidad de Valladolid

Facultad de Ciencias

Departamento de Física de la Materia Condensada, Cristalografía y Mineralogía

SYNTHESIS AND CHARACTERIZATION OF

AMPHIPHILIC ELASTIN-LIKE RECOMBINAMERS:

DEVELOPMENT OF SELF-ASSEMBLING

NANOPARTICLES AND HYDROGELS

A Master Thesis for the Degree of M.Sc. Molecular Nanoscience and Nanotechnology presented by

Sergio Acosta Rodríguez

Supervised by

Prof. Dr. José Carlos Rodríguez Cabello

AGRADECIMIENTOS

En primer lugar quiero dar las gracias a mi director de TFM, muchas gracias Carlos por dirigirme en este trabajo y por haberme dado la oportunidad de poder formar parte de este grupo.

También quiero agradecer a Javi y a todos los seniors; Matilde, Alessandra, Merche y Luis, toda la ayuda recibida desde el primer momento, y gracias a los cuales he podido aprender tantísimo.

A todos mis compañeros, muchas gracias por la atmósfera de trabajo de la que disfrutamos en el grupo, y por vuestra actitud, siempre dispuestos a ayudar en las dificultades que surgen en el día a día.

Por último quiero agradecer enormemente el apoyo de las personas que comparten mi día a día. A mis amigos, por estar ahí, por compartir conmigo tantos buenos momentos en este tiempo. A Cris muchas gracias por aguantarme, escucharme y apoyarme en todo momento. Y a mis padres y a mi hermana, mil gracias por creer en mí y porque sin vuestra confianza y apoyo nunca podría haber llegado hasta aquí.

A todos, muchas gracias.

Dans les champs de l'observation, le hasard ne favorise que les esprits préparés.

Louis Pasteur

CONTENTS

ABSTRACT

Nanotechnology is one of the science fields with a great development in the last years, with an imperative necessity to produce systems with specific functionalities at nanometric scale. Nanotechnology has provided sophisticated tools that have revolutionized many areas of knowledge, such as biomedical science, where enables improving efficiency and accuracy of current diagnostic techniques, and developing safer and more effective therapeutics[1].

In many cases, these systems are inspired by nature, trying to mimic nanometric structures formed by proteins and or other macromolecules in the living tissues and cells. Elastin-Like-Recombinamers (ELRs) are excellent candidates to develop systems that mimic the extracellular matrix structure due to their smart behavior and their recombinant nature. And they could be applied for instance, to develop treatments for connective tissue diseases as arthrosis.

The recombinant nature is one of the most important features of these polymers, that allows to produce them by recombinant expression in *Escherichia coli* from pre-designed genes. So we are able to design new materials with enormous potential that integrate new properties incorporated by genetic engineering for specific applications in nanomedicine.

The study shown here is focused on the development of new systems intended for injectable hydrogels in regenerative medicine, and for spherical nanocarriers in drug delivery. Based on the ability of self-organization into nanostructures demonstrated by previous amphiphilic tetrablock ELR[2], three new copolymers have been developed varying the individual blocks size, of the original tetrablock ELR. Thus, the aim of this investigation is to shed light about the influence of the block sizes on the physicochemical properties and on the structuration of the nanoparticles and of the hydrogels, with the final goal of setting the basis to perform a rational design from the sequence level.

RESUMEN

La nanotecnología es uno de los campos de la ciencia que mayor desarrollo ha experimentado en los últimos años, gracias a la necesidad imperiosa de producir nuevos sistemas con funciones específicas a escala nanométrica. La nanotecnología ha proporcionado sofisticadas herramienta, que han revolucionado múltiples áreas del conocimiento, como es el caso de la ciencia biomédica, donde ha permitido mejorar la eficiencia y la precisión de las técnicas diagnósticas actuales, y el desarrollo de terapias más efectivas y seguras[1].

Estos sistemas, en muchos casos, están inspirados en la naturaleza, intentan imitar las nanoestructuras formadas por proteínas u otras macomoléculas en tejidos y células vivas. Los Recombinámeros del tipo Elastina (ELRs) son unos excelentes candidatos para el desarrollo de sistemas que mimeticen la matriz extracelular debido a su comportamiento inteligente y a su naturaleza recombinante. Pudiendo ser empleados por ejemplo, para el desarrollo de tratamientos contra enfermedades del tejido conectivo, como la artrosis.

Su naturaleza recombinante es una de las principales características de estos polímeros, ya que permite su producción mediante expresión recombinante en *Escherichia coli* a partir de los genes pre-diseñados. Así, vamos a ser capaces de diseñar nuevos materiales con un potencial enorme que integre nuevas propiedades incorporadas a través de ingeniería genética para aplicaciones específicas en nanomedicina.

El estudio expuesto se centra en el desarrollo de nuevos sistemas pensados para su aplicación como hidrogeles inyectables en medicina regenerativa, y para su aplicación como nanotransportadores esféricos para liberación de fármaco. Basándonos en la capacidad de auto-organización en nanoestructuras demostrada por ELR tetrabloques anfifílicos previos, tres nuevos copolímeros han sido desarrollados variando el tamaño de los bloques individuales del ELR tetrabloque original. De este modo, el objetivo de esta investigación es arrojar luz sobre la influencia del tamaño de los bloques en las propiedades físico-químicas y en la estructuración de las nanopartículas y de los hidrogeles, con la finalidad de sentar las bases que permitan llevar a cabo un diseño racional a partir de la secuencia.

1 INTRODUCTION

1.1 Introduction to nanoscience and nanotechnology

Nanoscience is the study of the properties of matter at the nanoscale. Many research fields study these phenomena, like physics (e.g. quantum effects), chemistry (e.g. supramolecular chemistry; colloids, micelles, or polymer molecules) or biology and biochemistry (e.g. interactions in cell signaling, nanomachines)[3].

Nanotechnology arises from the knowledge derivate from Nanoscience, and is commonly defined as the understanding, control, and restructuring of matter on the order of nanometers to develop new materials with new or superior properties or functions[4].

Nanotechnology encompasses two main approaches:

- **The "top-down" approach** (physics) in which larger structures are reduced in size to the nanoscale while maintaining their original properties without atomic-level control (e.g., miniaturization in the domain of electronics) or deconstructed from larger structures into their smaller parts.

- **The "bottom-up" approach** (chemistry), in which materials are engineered from atoms or molecular components through a process of assembly or self-assembly. In this work, this approach has been used to get hydrogels based on cross-linked nanoparticles from individual protein chains.
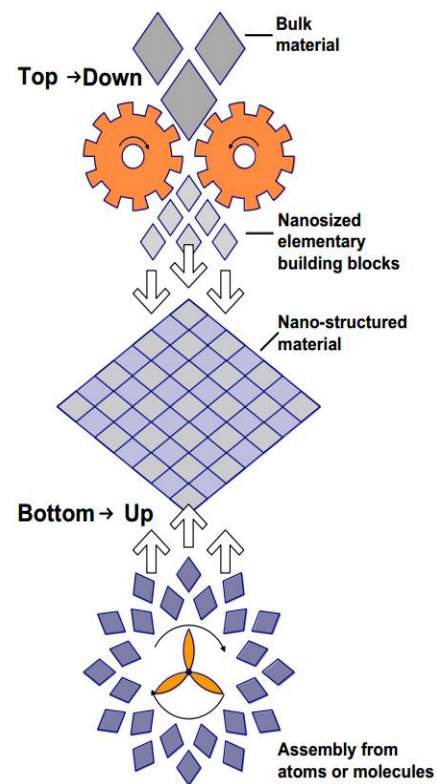
Figure 1 Illustration of the top-down and bottom-up approaches.

1.2 Protein based materials: ELASTIN-LIKE RECOMBINAMERS (ELRs)

Protein based-materials have drawn attention of numerous researchers in recent

years as promising advanced biomaterials for use in the field of biomedicine, especially as a result of recent improvements in recombinant DNA technology, which allow us to design and manufacture materials by exploiting the abilities of natural proteins[5]. Some of the most widely studied protein-derived materials are the so-called elastin like recombinamers (ELRs), taking into account its recombinant nature this new nomenclature was proposed[6] in replacement of the more conventional terminology elastin- like polymers (ELPs)[7-9], which include those first chemically synthesized materials.

1.2.1 Elastin-like recombinamers (ELRs)

Elastin is an elastic, insoluble protein that is widely distributed in vertebrate tissues, such as lung, skin, major vascular vessels, or tendon[10], where elasticity and resilience are a key requirement[11]. It is well-known for its extreme durability and ability to deform reversibly[12,13]. The origin of these properties reside in the structure of the recurrent sequences (VPGVG, VPGG, VGVAPG) found in the soluble elastin precursor tropoelastin[14].

ELRs are a family of repetitive artificial biopolymers all exhibiting a smart behavior. These polymers are a genetically engineered biomaterials inspired by natural elastin and the majority of its members are based on repeats of the pentapeptide sequence Val-Pro-Gly-Xaa-Gly, where Xaa is any natural amino acid except proline[15].

ELRs are a highly interesting biomaterials because their relevant characteristics. The natural elastin's mechanical properties are combined with other properties such as biocompatibility, stimuli-responsive behavior and the ability to self-assemble[16,17]. This class of smart polymers exhibits an inverse temperature transition (ITT) which allows them to undergo a reversible phase transition from a soluble to an insoluble state upon increasing or lowering the temperature above a specific threshold, the transition temperature (T_t)[15,18,19]. Below the T_t the polymer chains remain disordered in a relatively extended state with a random coil conformation, and fully hydrated[10]. This hydrophobic hydration is characterized by an ordered clathrate-like water structure surrounding the apolar moieties of the polymer (**Figure 2**). This structure is somewhat similar to that described for crystalline gas hydrates, although more heterogeneous and of varying perfection and stability[11,20]. When temperature surpasses the T_t, and according to Urry's model, the polymer chains hydrophobically fold and undergo a conformational transition

that leads to phase separation. That "coacervate" is composed of about of 63% water and 37% polymer[21]. In the folded state, the polymer chain adopts a dynamic, regular, non-random structure called β spiral, which involves one type II β turn per pentamer stabilized by intra-spiral inter-turn and inter-spiral hydrophobic contacts[6] (**Figure 2**).
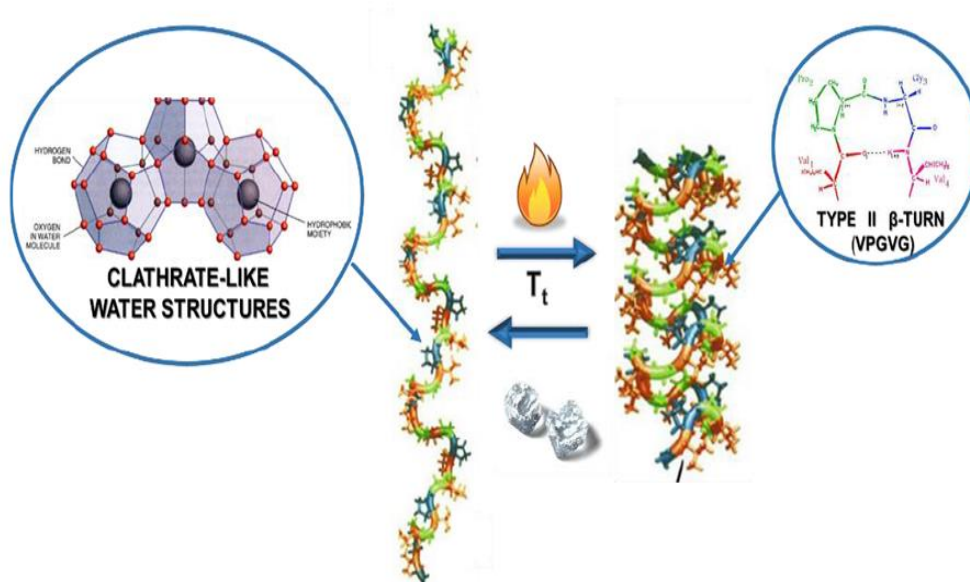
Figure 2: Schematic representation of the thermal transition of ELRs from an extended state (low temperatures, hydrophobic moieties surrounded by clathrate water structures) to a folded state (type II β-turn in VPGVG pentapeptides)

The process begins with the formation of filaments composed of three-stranded dynamic polypeptide β-spirals, which grow up to various hundred nanometers before settling into a visible separated state[6,14].(**Figure 3**)
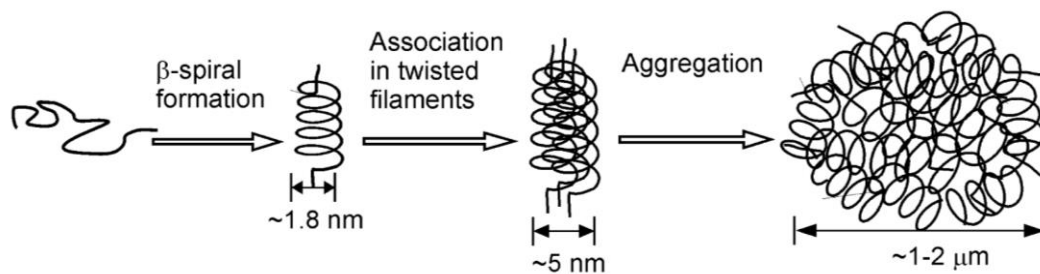
Figure 3 Mechanism of the ELRs' ITT. From left to right: β-spiral formation, formation of twisted filaments or β-spiral supercoil and their aggregation into microaggregates. Reproduced from reference[22].

Any modification in the composition of the polymer chain, intrinsic (sequence)

or extrinsic (adding a substance), will alter the clathrate structure and consequently will modify the T_t[23]. The ELP concentration and intrinsic factors like the modification of the guest residue, Xaa, and to a certain extent, the length of the polypeptide chain are factors that affect the transition temperature. The transition temperature can also be modulated by other physiological changes, such as changes in the pH, addition of extrinsic factors as salt, organic solutes or changing pressure[24].

Generally, T_t increases as the mean polarity increases and vice-versa. Additionally, if a chemical group that can be present in two different states of polarity exists in the polymer chain, and these states are reversibly interconvertible by appliance of an external stimulus, the polymer will exhibit two different T_t values[25,26]. This change in the T_t, opens a working temperature window in which the polymer isothermally and reversibly switches between the folded and unfolded states in response to environmental changes. This effect of changing the T_t is the basis of the ΔT_t mechanism and has been exploited to obtain pH, electric potential, light, chemical and other responsive interconvertible energy processes[25]. The hydrophobic paradigm, involving the ITT and the ΔT_t mechanism, for protein folding and function and the intrinsic capability of performing several energy interconversions allows new strategies for the development of ELP derivatives and working temperatures. Experimental studies on the ITT exhibited by ELPs and based on the factors that control hydrophobic folding and assembly of model proteins resulted in a set of five phenomenological axioms for the protein engineering of PBPs capable of inverse temperature transitions[27,28]:

- **Axiom 1**: The temperature intervals for the hydrophobic folding and assembly transition of a host protein or protein-based polymer with different guest substituents becomes a functional measure of their relative hydrophobicity.

- **Axiom 2**: Heating to raise the temperature from below, to above, the temperature interval for hydrophobic folding and assembly of macromolecules can drive contraction with the performance of mechanical work.

- **Axiom 3**: At constant temperature, an energy input that changes the temperature interval for thermally-driven folding and assembly in a

macromolecule can itself, drive hydrophobic folding and self-assembly at constant temperature.

- **Axiom 4**: Two or more different functional groups of a macromolecule, each of which can be acted upon by a different energy input that changes the temperature interval for hydrophobic folding and assembly, become coupled one to another by being part of the same hydrophobic folding and self-assembling domain, that is, the energy input acting on one functional constituent alters the property of another functional constituent as an energy output.

- **Axiom 5**: More hydrophobic domains make more efficient the energy conversions involving constituents undergoing conversion between more and less hydrophobic states.

1.2.2 Block Copolymers

Block copolymers have been the subject of numerous studies due to their ability to undergo self-assembled phase separation resulting in different complex morphologies. Self-assembly procedures have drawn attention over a number of years, with the self-assembly of nanoparticles being a particularly active field. Self-assembled polymer nanoparticles and hydrogels tend to be obtained from amphiphilic macromolecules. Generally speaking, a solution of these amphiphilic molecules in a solvent that only specifically solvates one part of the molecule will result in aggregation due to interaction of the solvent with the solvophobic blocks of the molecule. The hydrophobic parts tend to form aggregates as this collapse is more entropically favorable than the ordination of water molecules around each hydrophobic segment. On the other hand, hydrophilic parts are dissolve in water as the formation of hydrogen bonds with water molecules is higher enthalpic compensated than the interaction between hydrophilic parts.

1.2.2.1   Physical properties of Block Copolymers

Block copolymers are polymers composed of two or more covalently linked chemically distinct sequences (blocks).Thus, block copolymers can be designed as a hydrophobic block and a hydrophilic block, which can self-assemble into many different

structures[29].

The degree of order and morphology of those aggregates are dependent on concentration and volume ratio between the hydrophobic blocks and the hydrophilic blocks, known as insoluble soluble ratio (ISR). Below a certain concentration, critical aggregation concentration (CAC), the hydrophobic blocks are capable of maintaining the molecules dissolved. On the contrary, once above the CAC block copolymers begins to self- assembly resulting from the separation from the solvent of the hydrophobic block. The CAC decreases as the ISR and the molecular mass increases[30].

The dimensionless packing parameter (*p*) is the ratio between the molecular volumes of the solvent-phobic chain and the volume occupied by the copolymer in the assembly, defined as[29]:

$$p = \frac{v}{a_0 d}$$

Where a_0 is the optimal surface area of the solvent-phobic segment at the interface of between both blocks resulting from the balance between solvophilic solvophobic interactions, *v* is the volume and *d* is the length of the solvophobic block. Generally speaking, if $p \leq 1/3$ the self-assembled structure result in spherical micelles, while $1/3 < p \leq \frac{1}{2}$ correspond to cylindrical micelles and a p values between ½ and 1 are related to polymer membranes (**Figure 4**).

Theoretically speaking, the most stable assembly would be an infinity large membrane and an infinity long cylinder. Nevertheless, it goes without saying that the system is force to finite dimensions, thus a certain level of curvature (molecular frustration) is required in order to avoid the contact between the solvent and the insoluble parts[31].

Wormlike structures will come as a result of the stabilization by end-caps of cylindrical micelles if the molecular frustration is restricted to a specific part of the assembly. In the same way, under these local confinement of the molecular frustration, stabilization of membranes will consist on the curvature of the edges giving rise to disk-like micelles[32].
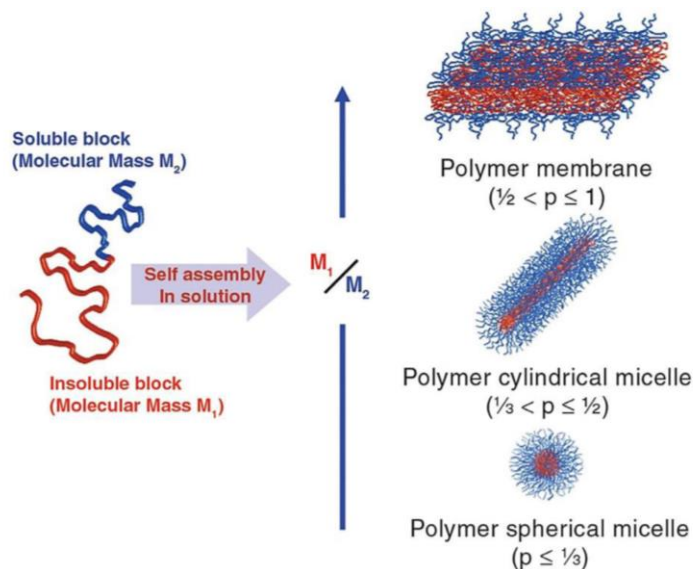
Figure 4 Different geometries formed by block copolymers in selective solvent conditions.

On the other hand, if all the molecules share the molecular frustration then stabilization of cylinders and membranes will result in the formation of toroidal micelles (as cylinders bend) and vesicles (membranes closure)

Energetically speaking, the formation of vesicles and worm-like micelles is more favorable than disk-like and toroidal micelles. But, it has been demonstrated that those less likely structures can be stabilized by the increase of the molecular mass of the copolymer[33,34], which will make the local frustration unfavorable, or by introducing extra interaction between block copolymers[35].

1.2.2.2 Protein-based block copolymers

Protein-based block copolymers consist of a type block copolymer in which some or all of the building blocks are composed by protein inspired materials, peptide sequences. Throughout the careful and specific selection and positioning of amino acid residues it is possible the production of polymers with an absolute control over the hydrophobicity patterns or secondary structures, which give rise to a wide selection of tailor-made materials[36].

As it has been previously described, see 1.2.2.1, the microstructure formation of synthetic block copolymer is highly influence by the ISR, but the phase separation parameters are not the only factors influencing the structure formation when it comes to

protein-based block copolymers. When dealing with protein inspired materials, intra and inter-molecular bonding, together with chain conformation, are to be taken also into account in the process of structures formation. Thus, a different phase behavior from that of synthetic block copolymers should be expected, mainly due to normally occurring interactions in protein, such as electrostatic interactions, peptide backbone rotational restrictions, high hydrogen bonding or hydrophobic interactions, are usually absent from the synthetic block copolymer systems. The supramolecular organization in proteins is mostly directed by two structural elements, α-helix and β-sheet. All in all, the conditions under which structures (microphase separation) self-assemble and subsequence phase diagram relationships is yet to be determine for most of protein-based copolymers. Protein-based block copolymer can be divided into two main groups; synthetic polymer-peptide block copolymer (hybrids) and protein/peptide block copolymers.

1.2.2.3   Elastin-Like block co-Recombinamers (ELbcRs)

Recent advances in recombinant DNA techniques have provided the tools needed to produce block corecombinamers with the desired sequence, depending on the application, from simple amino acids with an absolute degree of control and complexity superior to those of synthetic polymers.

Amphiphilic elastin-like block co-recombinamers (ELbcRs) can form nano- or micro-sized structures[37,38] To this end, ELR-based amphiphilic tetrablock copolymers have been synthesized in which the amphiphilicity of the component blocks is achieved by substituting the amino acid (X) in the guest position of the pentamer VPGXG by a hydrophilic (glutamic acid), or hydrophobic (isoleucine) amino acids. Nanoparticle formation occurs when the elastin-like block co-recombinamer (ELbcRs) solution is heated above the characteristic Tt of the hydrophobic block, at which point the co-recombinamer chains organize themselves by hiding the hydrophobic blocks from the aqueous environment, thus reaching a minimum free energy situation.

Mean polarity, molecular weight, amino-acid sequence and molecular architecture are parameters influencing the final morphology and size of the final nano-assemblies, which have been demonstrated to assemble into micelles or hollow vesicles[39].
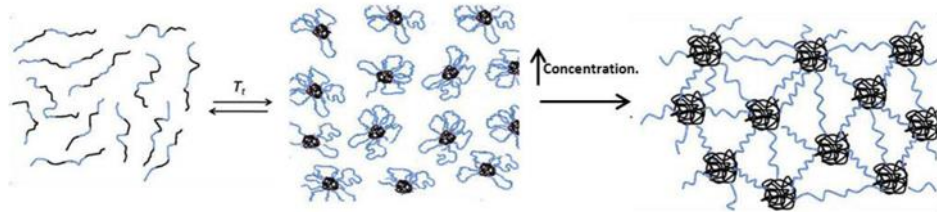
Figure 5 Schematic representation of the formation of a physical hydrogel through the micellation of a tetra-block ELR. Below Tt the monomers are extended, once above Tt the hydrophobic block (black) aggregates forming nanoparticles. If the concentration is increased that aggregation leads to the formation of a water swollen network resulting in the hydrogel formation.

ELbcRs have also been reported as materials capable of forming physical hydrogels at a sufficiently high concentration. In this sense, tetrablocks (polar-apolar-polar-apolar) has been reported to self-assemble into a physical hydrogel once above the T_t. These materials are designed to be injectable self-gelation systems with high applicability in biomedical applications, such as tissue repair or as drug delivery systems for local therapies. In order to fulfill the requirement of injectability the material is required to be a low viscosity liquid below the physiological temperature. In this sense, the monomers are completely unassociated in aqueous solution below the T_t and once above the T_t the hydrophobic elastin domains undergo a phase separation associating into micellar aggregates acting as virtual cross-links (**Figure 5**).

2 MATERIALS AND METHODS

2.1 MATERIALS

2.1.1 Chemical Reagents

All the reagents employed on this work are listed on **Table 1**

Reactive	Brand
Acrylamide/Bis-acrylamide	Amresco
Agarose Seakem.	Cambrex
Ammonium persulphate (APS).	Sigma-Aldrich
Ampicillin	Apollo Scientific
Bromophenol blue	Sigma-Aldrich
Chloridric acid	Merck
Copper chloride	Sigma-Aldrich
Dimethyl sulfoxide (DMSO)	Carlo Erba
Ethanol	Merck
Glycerol	Sigma-Aldrich
Glycine	Sigma-Aldrich
Mineral oil	Sigma Aldrich
Phenylmethylsulfonyl fluoride (PMSF).	Apollo Scientific
Phosphate buffered saline (PBS)	Gibco
Sodium chloride (NaCl)-	Sigma-Aldrich
Sodium dodecyl sulfate (SDS)	Sigma-Aldrich
Sodium hydroxide	Sigma-Aldrich

Tetramethylethylenediamine (TEMED).	Sigma-Aldrich
Ultrapure water	Millipore
β-Mercaptoethanol.	Sigma-Aldrich

Table 1 Reagents employed and suppliers.

2.1.2 Other materials

During the realization of this work light scattering techniques have been employed, where glass test tubes were used. The contamination of such tubes with organic residues, dust or grease may interfere with the results obtained, being necessary to pay special attention to the cleaning of the tubes employed. An optimum cleaning is achieved by rinsing the tubes out with distilled water followed by a wash with a mixture soap-water (Hellmanex ®II special for optical cleaning). To remove soap traces the tubes are extensively washed with water. Finally, the tubes are rinsed with water type I and allowed to dry in an oven at 60°C for at least 4 hours.

Other glass materials after washing and rinsing several times with distilled water were sterilized on an autoclave (Autotester E-75). Other laboratory materials like tips, conical tubes, Eppendorf tubes, falcon tubes, etc. are bought sterile or are sterilized when needed on an autoclave (Autotester E-75, 20 minutes 120°C one atmosphere).

2.1.3 Molecular biology materials

2.1.3.1 Restriction enzymes

The restriction enzymes used in this work are listed below:

DpnI, EarI, EcoRI, SapI, XbaI, XhoI (Thermo Fisher).

All enzymes are used according to the manufacturer instructions.

2.1.3.2 Other enzymes

The following enzymes have been employed, being all of them purchased to Thermo Fisher and used under the suggested conditions:

2.1.3.3 Cloning and expression vectors

The DNA fragments employed were cloned in pDrive cloning vector (Qiagen), **Figure 6**.

pDrive Cloning Vector

Positions of various elements

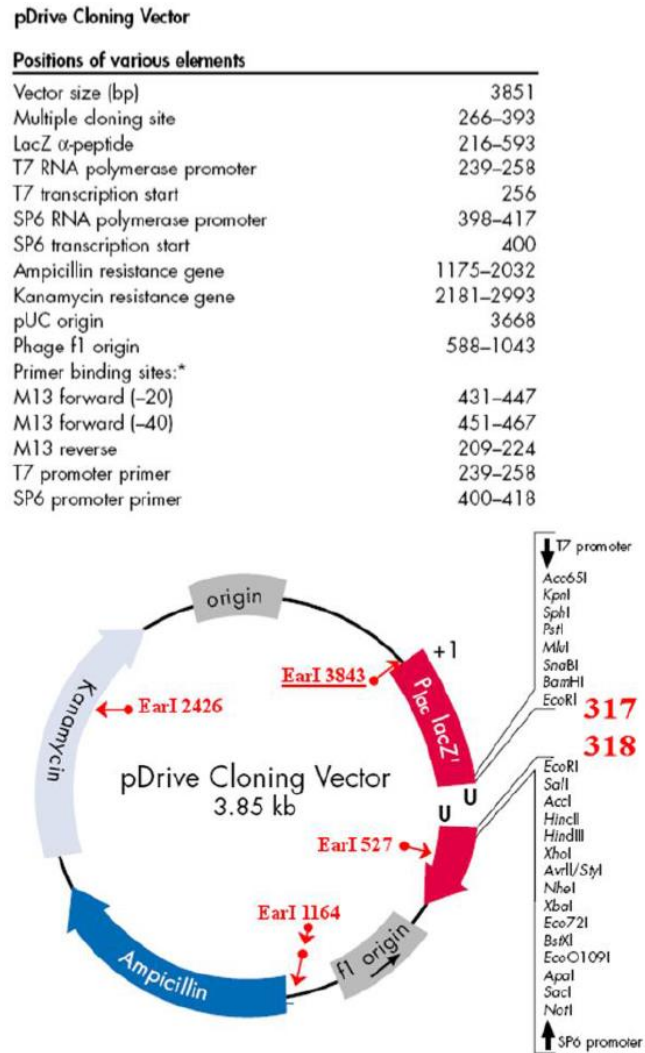|	
Vector size (bp)	3851
Multiple cloning site	266–393
LacZ α-peptide	216–593
T7 RNA polymerase promoter	239–258
T7 transcription start	256
SP6 RNA polymerase promoter	398–417
SP6 transcription start	400
Ampicillin resistance gene	1175–2032
Kanamycin resistance gene	2181–2993
pUC origin	3668
Phage f1 origin	588–1043
Primer binding sites:*	
M13 forward (–20)	431–447
M13 forward (–40)	451–467
M13 reverse	209–224
T7 promoter primer	239–258
SP6 promoter primer	400–418

Figure 6 pDrive cloning vector (Qiagen).

For the expression of the different recombinant polimers a p7 expression vector has been employed **Figure 7**. The p7 expression vector was constructed in our laboratory from Novagen's pET-25b (+) vector, by Dr. A. Girotti.
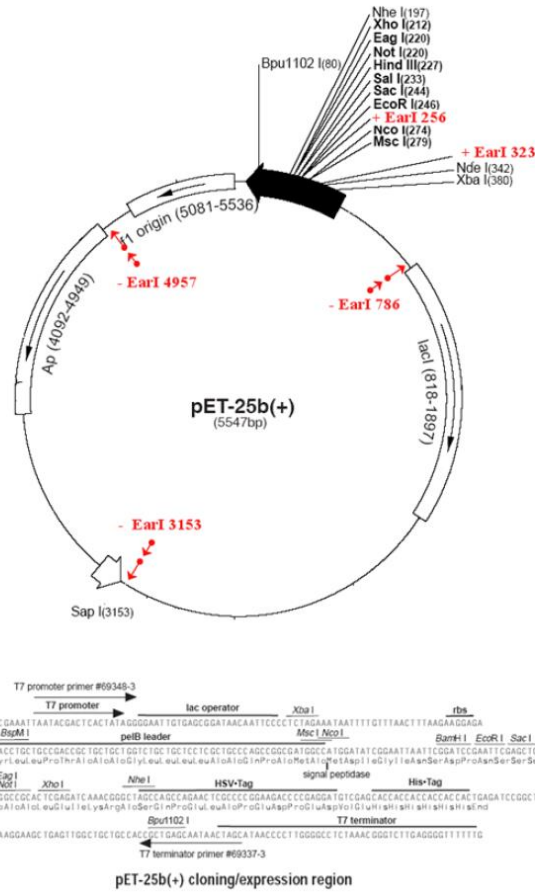
Figure 7 Scheme of p7expression vector based on Navagen's pET-25b(+) vector

2.1.3.4 Other reagents

Two kits were used for the plasmid and DNA purification either from an Escherichia coli (*E.coli*) culture: NucleoSpin Plasmid (Macherey-Nagel) and Quantum Prep Plasmid Midiprep Kit (Bio-Rad); or from an agarose gel: PureLink Quick Gel Extraction Kit (Life Technologies).

2.1.4 Bacterial strain

The *E. coli* strains used on this work have the following genotypes:

a) **XL1-Blue Competent Grade/Subcloning Grade** (Stratagene): endA1 supE44 hsdR17 thi1 recA1 gyrA96 relA1 lac [F' proAB lacI$_q$ ZΔM15 Tn (Tet$_r$)].

b) **BL21 (DE3) Star** (Novagen): F- ompT hsdSB (r$_B$- m$_B$-) gal dcm (DE3) 127.

c) **BLR (DE3)** (Novagen): F- ompT hsdSB (rB- mB-) gal dcm Δ (srl-recA) 306::Tn10 (Tetr) (DE3).

2.1.5 Culture media

The culture media used for bacteria growth and transformation are listed below:

a) **Luria-Broth (LB)** (Pronadisa): Concentration 25g/L.

b) **Terrific Broth (TB)** (Formedium): 55.85 g/L + 8mL/L Glycerol.

c) **LB-Agar**: LB 25 g/l + 1.5 % (p/v). Agar (Fluka).

d) **SOC Broth**. (Sigma Aldrich).

2.1.6 Buffers

During the performance of the work presented on this thesis different buffers were employed:

a) **PBS** (pH=7,4): 5mM, NaCl 137 mM, KCl 2.7 mM, 10mM Na2 HPO4 , KH2PO4 1.8 mM

b) **TAE**: 40 mM Tris-acetate, 1mM pH=8 EDTA.

c) **TE** (sonication buffer): 10 mM pH 8 Tris-base, 1 mM pH=8 EDTA, 1mM PMSF.

d) **TBS** (washing buffer):20 mM pH 8 Tris-base, 140 mM NaCl.

e) **Running buffer**: Tris-base 25 mM pH=8,3, glicina 192 mM y SDS 0,1% (w/v).

f) **DNA loading buffer**: 30% (v/v) glycerol, 0.1% (w/v) SDS, 0.05% (w/v) bromophenol blue (BPB), 50mM Tris pH 8, 0.05mM EDTA.

g) **Protein loading buffer**: Tris 1MpH 6.5 312.5 mM, SDS 10%(w/v), Glycerol (v/v), β-Mercaptoethanol 25%(v/v), bromophenol blue (BPB) 2% (v/v).

All the solutions were prepared using ultrapure type I water (Millipore).

2.1.7 Elastin-like recombinamers (ELRs)

All the elastin-like recombinamers (ELRs) employed in the development of this work have been designed and produced in our laboratory (G.I.R. Bioforge) by recombinant DNA techniques. Those recombinamers have been specifically designed for the realization of this work, and these have been produced by E. Coli fermentation and purified taking advantage of both the smart nature and the reversible thermo-dependent segregation showed by this kind of materials, by inverse transition cycling (ITC)[8].

DNA corresponding the individual blocks E50, I40 and I60 were cloned by Dr. García-Arévalo, while the gene of the amphiphilic tetrablock (E50I60)2 was constructed by the Dr. Martín Maroto. Despite that, I reconstructed this tetrablock to verify the sequence. Also three new amphiphilic tetrablocks were constructed. Table 2 shows all the tetrablocks employed, the abbreviation, molecular weight (Mw), and amino acid sequence.

Elastin-like recombinamer (ELR) abbreviation	Amino acid sequence	Molecular weight (Mw)
$(E50I60)_2$	MESLLP $$[[(VPGVG)_2\text{-}VPGEG\text{-}(VPGVG)_2]_{10}$$ $$(VGIPG)_{60}]$$ V	93157.7 Da

E100I60E50I60	MESLLP $[(VPGVG)_2\text{-}VPGEG\text{-}(VPGVG)_2]_{20}$ $(VGIPG)_{60}$ $[(VPGVG)_2\text{-}VPGEG\text{-}(VPGVG)_2]_{10}$ $(VGIPG)_{60}$ V	113931.8 Da
E50I60E50I100	MESLLP $[(VPGVG)_2\text{-}VPGEG\text{-}(VPGVG)_2]_{10}$ $(VGIPG)_{60}$ $[(VPGVG)_2\text{-}VPGEG\text{-}(VPGVG)_2]_{10}$ $(VGIPG)_{100}$ V	110098.20 Da
(E50I100)₂	MESLLP $[[(VPGVG)_2\text{-}VPGEG\text{-}(VPGVG)_2]_{20}$ $(VGIPG)_{100}]_2$ V	127038.7 Da

Table 2 Amino acid composition and molecular weight of the elastin-like recombinamers used.

2.2 METHODS

2.2.1 DNA agarose gel electrophoresis

DNA agarose gel electrophoresis are used to separate and check the appearance and size of DNA fragments form either a plasmid or from an enzymatic digestion with endonucleases. Different concentrations (in 1x TAE), are applied according the sizes of the DNA fragments and the kind of gel, analytical or preparative, being the first one used to assess the rightness of a purified plasmid and the second one to obtain DNA for further use. The different agarose concentrations and their resolution capability are listed in the **Table 3**.

Fragment size (bp)	Agarose final concentration (% 1x TAE)
800-10000	0.8
400-8000	1
300-7000	1.2
200-4000	1.5
100-2000	2

Table 3 Resolution for linear DNA in electrophoresis of different agarose gel concentrations.

The gels are prepared adding in a glass-made Erlenmeyer flask the quantity of agarose and a volume of buffer according to the gel concentration and size. The agarose is melted on the microwave, after weight and hydration, until the formation of a gel. Once melted, the flask with the gel is weighted again and ultrapure deionized water is added until reach the initial weight, maintaining the initial concentration and gel uniformity.

After cooling down to 60ºC the gel is casted in a horizontal tray with the desired comb.

The samples are applied adding 0.2 volumes of 5x loading buffer. A fixed voltage, between 2 and 7 V/cm – according to each sample, is then applied. The electrophoresis is run having as references the color markers (**Table 4**). Last, the gel is stained for 10 to 30 minutes in a 1x GelRed™ solution, and the DNA bands are visualized by exposition to UV light in a Viber Lourmat, TFX-20M transilluminator.

TAE 1x –BPB	% Agarose
2900	0.30
1650	0.50
1000	0.75
500	1
370	1.25
200	1.75
150	2

Table 4 Relation between linear DNA migration and bromophenil blue (BPB).

2.2.2 Plasmid purification

The plasmids employed in this work were purified, using the commercial systems listed above, following the manufacturer's instructions. DNA was eluted with ultrapure water or Elution buffer from the kits. For applications where higher DNA concentration is required only half of the recommended elution volume is used, the elution water is used at 65°C and the time incubation was increased up to 10 minutes to enhance the purification yield. The eluted DNA is stored under -20ºC.

2.2.3 DNA digestion with restriction enzymes

Reaction conditions (temperature, concentration, time of reaction, buffer) for the digestion are supplied by the enzyme manufacturer. The rate of digestion is controlled by DNA agarose gel electrophoresis.

2.2.4 DNA dephosphorylation

Dephosphorylation reaction conditions (temperature, time of reaction, buffer) are supplied by the phosphatase manufacturer. For the p7 expression vector two different consecutive phosphatases were used and the incubation time was enlarged until one hour.

2.2.5 DNA fragments purification from an agarose gel

The target DNA band is first separated and visualized in an analytic agarose gel of an appropriated concentration and stained with GelRed™Nucleic Acid (as indicated in 2.2.1), secondly, the band is extracted from the gel with the help of a scalpel. Minimum quantity of agarose should be cut during band extraction.

The purification of the fragment is carried out using the commercial system "PureLink Quick Gel Extraction Kit" (Life Technologies), following the protocol indicated by the manufacturer.

2.2.6 Ligation reaction

The reaction ligation is carried out in a final volume of 15μL by mixing the insert with the vector, in a molar relation from 1:1 to 5:1, and T4 DNA ligase as enzyme with its corresponding buffer following the specifications indicated by the supplier. The reaction is conducted during 1 hour at room temperature or during 24 hours at 4°C.

2.2.7 Cloning on the pDrive/ p7 vector

The ligation reaction is interrupted by the inactivation of the T4 DNA ligase by incubation during 10 minutes at 70°C. Once the ligation reaction is concluded, a certain quantity of it is used to transform competent cell as specified below.

2.2.8 Transformation of competent cells

2.2.8.1 Transformation of XL1 blue subcloning grade competent cells

This bacterial strain has an efficiency $\geq 10^6$ transformants per μg of DNA. Plasmid DNA to be amplified by cloning is transformed in this bacterial strain following the protocol specified by the supplier.

2.2.8.2   Transformation of XL1 blue competent cells

This bacterial strain has an efficiency $\geq 10^8$ transformants per μg of DNA. Ligation products were transformed into this bacterial strain following the protocol specified by the supplier.

2.2.8.3   Transformation of BLR (DE3) competent cells

This bacterial strain is transformed with the expression plasmid p7 following the method TSS reagent ("Transformation and Storage Solution")[40]. This method is a combination of two steps from the transformation procedure, first we obtained competent cells and second the cells are stored at -80ºC or transformed resulting in transformation efficiency that goes up to the 10^7 cfus (colony forming units) per microgram of DNA.

A single colony, isolated and grown in a LB-agar plate, is used to inoculate 100 mL of LB medium (plus antibiotic) and is grown at 37ºC with shaking (250rpm), until reach a OD_{600}=0.3-0.4. At this point the metabolism and cell growth is stopped by incubation on ice for 5 minutes. The cell suspension is centrifuged at 3000rpm (1100Gx) for 10minutes at 4ºC. The supernatant is discarded and the pellet is re-suspended in 10mL of cold 1xTSS solution, and is mixed gently (TSS1x is LB broth containing 10% (wt/vol, Mw 8000) polyethylene glycol, 5% (vol/vol) dimethyl sulfoxide, and 50 mM Mg^{2+} at pH 6.5) Now the competent cells are ready to be transformed. 150 μL competent cells are aliquoted to 1.5 mL Eppendorf tubes and are storage at -80ºC (pre-treated with liquid nitrogen).

At the moment of the transformation, an aliquot is defrosted in ice, and about 1-10 ng of plasmid in final volume of 1-10μL are added to the mix. The cellular suspension plus the plasmidic DNA are kept on ice thirty minutes. A 0.85 ml of pre-warmed LB is added and the suspension is incubated one hour at 37ºC with shaking (250rpm). And finally, 50-200 μL of the transformation mix is plated in LB-agar plus the antibiotic plates that are incubated for 16-20 hours at 37ºC.

2.2.9   Glycerol stock preparation

To maintain and store the clones with interest, glycerol stocks were made. The selected colonies (by SDS-PAGE electrophoresis) are grown at 37°C with shacking

(250rpm.) on LB or LB with 0.5% of glucose (for the expression strains) plus antibiotic, until reaching an OD600= 0.6-0.8. At this point 0.1 volumes of 80% sterile glycerol are added and the cells are added to a cryovial and are stored at -80°C.

2.2.10 DNA Sequencing

The automatic DNA sequencing was made at Cenit Support Systems S.L.L.-Scientific park of Salamanca (Villamayor, Salamanca).

2.2.11 Production and purification of recombinant polymers

2.2.11.1 Recombinant polymer's expression

During the biosynthesis of the four different tetrablocks employed in this work the expression vector p7 has been employed. p7 has been obtained in our laboratory by mutagenesis of pET25b (+) by Dr. Alessandra Girotti. The final constructions were transformed on the bacterial strain BLR (DE3) following the above mentioned protocol (see 2.2.8.3).

ELRs expression starts inoculating the desired colony in liquid LB medium plus antibiotic and 1% of glucose at 37 °C with orbital shaking (250 rpm.) during approximately 6 hours. This culture is used as inoculum for a fresh TB medium (plus antibiotic), in a volume ratio of 1:500, not exceeding the 25% of the capacity of the Erlenmeyer used. This culture is grown for 14-16 hours at 37 ° C with orbital shaking (250rpm.).

For large batches production, as this case, a 15L Bioreactor is used (Applikon Biotechnology), allowing the full control of variables like temperature, pH, OD600 and oxygen concentration, regulating all of them if needed, improving the yield of the bioproduction process. It is inoculated with 1L of the pre-incubated cell suspension to a final volume of 15L of TB medium and fermentation time varies from 14 to 16h, setting temperature at 37ºC, pH at 7, oxygen control at 50% of the initial oxygen concentration and stirring at 499rpm.

2.2.11.2 Bacteria disruption

Once the induction is finished, the bacteria's metabolism and growth are stopped

by cooling it down to 4ºC and cells are centrifugated and washes with Washing buffer (see 2.1.6) until having a clear supernatant. Then the pellet is re-suspended in a volume V_{TE} of TE per liter of culture (see 2.1.6):

$$V_{TE}=5*V_{culture}*OD_{600}$$

Cell suspension is kept at 4ºC and 10µg/mL of PMSF protease inhibitor is added.

Bacteria are disrupted (lysated) by changing pressure disruption employing a Constant Cell Disruption System (Model TS 0.75KW, Constant System). Finally, the lysate is centrifuged at 4ºC for 60 minutes at 15000xg. The supernatant contains the recombinant polymer biosynthesized.

2.2.11.3 Purification of the recombinant protein-based polymer

The purification of ELRs starts from the supernatant obtained at the end of the lysis process (see 2.2.11.2), taking advantage of the ELRs' smart nature and inverse temperature transition (ITT). Therefore, the purification process is based on successive cycles of precipitation (heating) and resuspension (cooling) of the supernatant, named Inverse Transition Cycling (ITC).

The ELRs biosynthesized in this work had glutamic acid residues in their sequence (see **Table 2**), which at a pH above its pKa are depronated and therefore negatively charged what increase significantly their T_t[41]. In order to reduce the T_t and in this sense, facilitate the precipitation of the ELRs, NaCl is added during the purification process until a 2M concentration is achieved.

Finally, after the last purification cycle, the re-suspended polymer is dialyzed against cold ultrapure type I water. The suspension is then adjusted to pH 7, passed through a 0.2 µm PES (Polyethersulphone) filter, and lyophilized and stored at -20°C. Purification steps, as well as the final product, are checked by polyacrylamide gel electrophoresis.

2.2.12 Denaturing polyacrylamide gel electrophoresis

The protein polyacrylamide gel electrophoresis in the presence of sodium dodecyl sulfate – SDS-PAGE – is made following the protocol for discontinuous systems

described by Laemmli[42] to accomplish the separation of a proteins mixture by their molecular weight, being the gel composed of two different sub-gels: stacking and resolving.

There are almost no differences between the proteins' effective charge because the SDS strongly interacts with proteins providing them with approximately one negative charge per each amino acid residue. The denaturing conditions are obtained because the SDS denatures the quaternary and tertiary structure of the proteins by breaking the non-covalent interactions. Besides, β-mercaptoethanol (a reducing agent) is added to the samples in order to break the disulfide bonds that might exist. This process is facilitated with the heating of the samples during 5 minutes at 95ºC.

A "MiniVE vertical electrophoresis system" from Hoefer (Amersham Pharmacia Biotech, Pittsburg, USA) electrophoretic system was employed to perform the polyacrylamide electrophoresis. The total percentage of acrylamide (%T) in the resolving gel varies according to the molecular weight of the polypeptide we want to separate. The optimal %T for a determined size range is presented in **Table 5**.

Target size range (kDa)	%T in resolving gel
24-205	7.5%
14-205	7.5%
14-66	12.5%
14-45	15%

Table 5 Optimal %T according to the polypeptide target size range.

The composition of a resolving and stacking for a gel X%T is detail in **Table 6**.

Reactive	Resolving gel	Stacking gel
Acrylamide 40%	10% (w/v)	4% (w/v)
Tris-HCl pH 8.8	375 mM	--------
Tris-HCl pH 6.8	--------	125 mM
SDS 10%	0.1% (w/v)	0.1% (w/v)
APS 10 %	0.05% (w/v)	0.05% (w/v)
TEMED	0.05% (w/v)	0.08% (w/v)

*both gels are prepared in ultrapure type I water

Table 6 Composition of the resolving and stacking gel in a gel 10%T.

A molecular weight marker (Unstained Protein Molecular Weight Marker,

Thermo Fisher) is loaded together with the samples in order to know the molecular weight of each band[43]. Staining is performed according to Lee's method[44]: Ten minutes incubation at room temperature of the gel in a 0.3M Copper chloride solution followed by a washing step in distilled water for 5 minutes. Pictures are taken by 'Gel Logic 100 Imaging System' camera system and 'Kodak 1D Image Analysis (Kodak)' software.

2.2.13 Experimental techniques

2.2.13.1 Dynamic light scattering

Dynamic light scattering (DLS) is a technique for measuring the size of particles normally in the sub-micron region. Typically, DLS is concerned with measurements of dispersed particles or suspended macromolecules in a liquid medium, measuring the particles Brownian motion and relating it to the particles' size.

Brownian motion is the random movement of particles suspended in a fluid due to their collision with the solvent molecules that surround them. Thus, the random motion will be affected by different factors, mainly the size of the molecules (the bigger the molecules, the slower they move), the viscosity of the solvent (the more viscous the solvent, the slower the molecules move) and temperature. Temperature is a crucial parameter, both temperature stability and temperature accurate knowledge are required, due to its influence on the solvent viscosity and owing to, temperature instability will lead to convection currents in the sample, thus non-random motion, resulting in incorrect size interpretation.

The velocity of the Brownian motion is defined by the translational diffusion coefficient (D), which is used to calculate the size of the particles by using the Stokes-Einstein equation:

$$D_h = \frac{k_B T}{3 \pi \eta D}$$

Where k_B is the Boltzmann constant, T is the temperature and η is the viscosity. It is worth noting, that DLS refers to how a particle diffuse within a fluid so the calculated diameter is a hydrodynamic diameter (D_h), (effective molecule diameter + hydration layer, **Figure 8**)
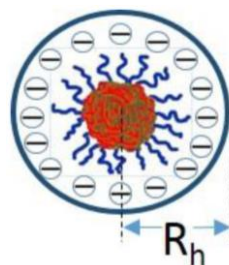
Figure 8 Representation of particle with its hydration layer, hydrodynamic radius.

Light scattering measurements were performed using a Zetasizer nano ZSP (Malvern instruments) equipped with a 10 mW He-Ne laser at a wavelength of 633 nm.

2.2.13.2 Zeta potential

Z-potential analysis is a technique for determining the surface charge of nanoparticles in solution. The Z-potential of the ELR was monitored at 37°C using a Zetasizer nano ZSP apparatus (Malvern instruments). The Z-potential values, which were determined using the Smolukowski equation relating ionic mobility to surface charge, were plotted as the average of 10 repeated measurements.

2.2.13.3 Differential scanning calorimetry (DSC)

Differential scanning calorimetry (DSC) is a technique in which the difference in the amount of heat required to increase the temperature of a sample and reference is measured as a function of temperature.

DSC experiments were performed on a Mettler Toledo 822e with liquid-nitrogen cooler. Both temperature and enthalpy are calibrated with a standard sample of indium. The solutions for the DSC experiments were prepared at 50 mg/mL in water or an aqueous buffered solution (PBS). 20 μL of the solution were placed inside a standard 40-μL aluminum pan and sealed hermetically. The same volume of the employed solvent was placed in the reference pan. Both, sample and reference are heated at a constant velocity.

The heating program included an initial isothermal stage (5 min at 0º C for stabilization of the temperature and the state of the polymers), followed by heating at 5º C/min from 0º C to 60ºC.

2.2.13.4   Rheology

Rheology is the study of flow and deformation of materials under applied forces. In this sense, it was used to analyze the thermogelification process of the different tetrablock-ELRs, by studying their mechanical properties in order to obtain the storage and loss moduli of the hydrogel.

Trhe viscoelastic properties of 250, 275 and 300 mg/mL solutions (final volume of 300µL) of each tetrablock-ELRs in ultrapure water and in PBS buffer were evaluated using a controlled stress rheometer (AR-2000ex, TA Instruments). A 12 mm Standard steel parallel plate was used to characterize the rheological properties at a constant strain of 0.3% and a frequency of 1 Hz, mineral oil was used at the edge of the samples to prevent solvent evaporation in the hydrogels.

To characterize the gelation kinetics of the tetrablock-ELRs hydrogels, time-sweep experiments were performed at 25ºC and 37ºC Strain sweeps were carried out across a strain range of 0.01-15%. Temperature ramps were performed from 5ºC to 40ºC (heating rate: 5ºC/min).

2.2.14 Experimental techniques performed by external services

2.2.14.1   Amino-acid analysis

The amino acid composition of the ELRs employed during this work was determined by *Laboratorio de Técnicas Instrumentales (University of Valladolid)*.

After addition of a known quantity of α-aminobutyric acid as internal pattern the samples were hydrolyzed (6M HCl, 1% Phenol and 2.5 hours at 155°C) and evaporated. The powder was resuspended in 1mL of 20mM HCl and a 1/10 dissolution was prepared. The quantification of the less represented amino acids was made from the most concentrated sample and the quantification of the most represented amino acids from the 1/10 dissolution. One aliquot of each dissolution was derivatizated according to the AccQ-Tag Waters method and analyzed by HPLC with UV detection, using a WATERS600 HPLC gradient system with a WATERS2487 detector.

2.2.14.2   MALDI-TOF Mass Spectrometry Analysis

Determination of the ELRs molecular weight was made by MALDI TOF at the

Laboratorio de Técnicas Instrumentales (University of Valladolid).

2.2.14.3 Cryo-Transmission electron microscope (Cryo-TEM)

(Cryo-TEM imaging acquisition of buffered solutions was performed at CIC bioGUNE Structural Biology Platform, Bilbao).

Samples were prepared through rapid vitrification of the liquid samples in the automated vitrification robot Vitrobot™ Mark IV (FEI).The specimens were observed with a JEM-2200FS/CR transmission electron microscope (JEOL, Japan), equipped with an ULTRASCAN 4000 SP (4008×4008 pixels) cooled slow-scan CCD camera (GATAN, UK).

3 RESULTS AND DISCUSSION

3.1 DESIGN, CONSTRUCTION AND RECOMBINANT PRODUCTION

The use of block copolymers in nanotechnology has acquired a great interest in the last years. They enable the possibility of creating different structures in the nanometer scale thanks to their self-assembly properties in an easy and non-expensive way using the *bottom up* approach[45].

In this study, to facilitate the rational engineering of the physico-chemico properties of hydrogels based on amphiphilic tetrablock ELRs, three new tetrablock recombinamers with different molecular weight and composition were designed, taking as point of departure, the amphiphilic tetrablock E50I60E50I60 (**A** in **Figure 9**). A recombinamer that is comprised by two hydrophilic blocks, L-Glutamic acid containing block (E-block) and two hydrophobic blocks, L-Isoleucine containing block (I-block).

The identity and sequence of the individual block units within the polymer dictates the nature of the supramolecular assembly, for this reason two of the new tetrablocks incorporated an extra-block at the N-terminal end (**B** in **Figure 9**) and at the C-terminal end (**C** in **Figure 9**). Thus, the influence of an 'asymmetric' block could be evaluated.

Figure 9 Scheme of the four different tetrablock ELR sequences.

And finally, a tetrablock ELR that incorporated an extra hydrophobic content preserving the proportionality between its two diblocks was also designed (**D** in **Figure 9**).

The construction of the different genes was performed following the guidelines described in material and methods. The different tetrablock genes were constructed on pDriveAll vector starting from the individual blocks E50, I40 and I60. All the constructions were assessed by agarose gel electrophoresis in every step of the process and by DNA sequencing. **Figure 10** and **11** show the results of the different steps of the genetic engineering process. **Figure 10** presents the starting building blocks in the cloning plasmid pDriveAll (Lanes 1-3) and the diblocks constructed as a middle point before obtaining the final tetrablocks (**Figure 11** shows the desired tetrablock ELRs in the expression plasmid p7).
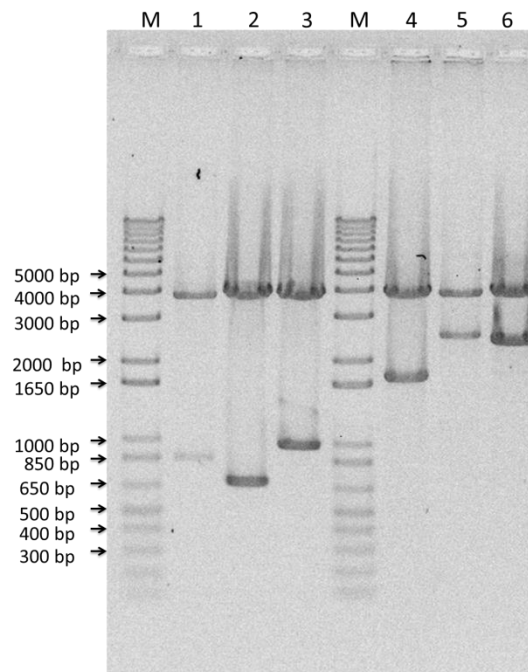

Figure 10 Enzymatic analysis with the *Eco*RI endonuclease of the colonies containing the plasmid pDrive All and the inserts: Lane 1: E50 (750 bp); Lane 2: I40 (600 bp); Lane 3: I60 (900 bp); Lane 4: E50I60 (1650 bp); Lane 5: E100I60 (2400 bp); Lane 6: E50I100 (2250 bp); Lanes M: DNA marker 1Kb Plus.DNA agarose.

The digestion with *Eco*RI produced two bands, an upper band corresponding to the pDrive plasmid and a lower one corresponding to the insert plus 100bp.
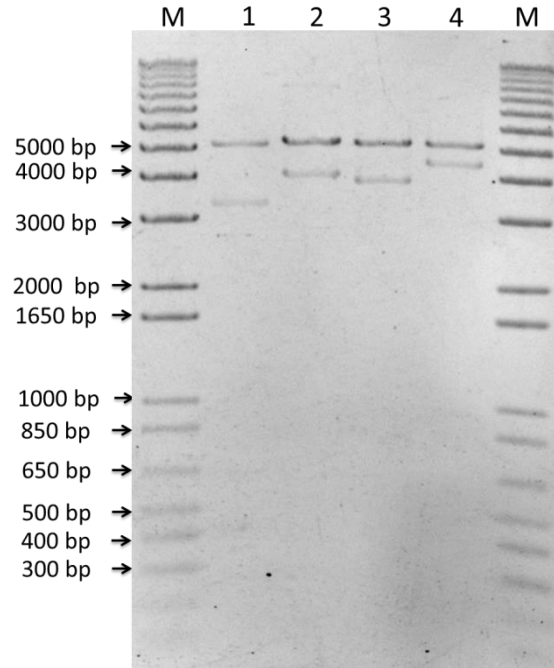
Figure 11 Enzymatic analysis with the *Xho*I and *Xba*I endonucleases of the colonies containing the expression plasmid p7 and the inserts: Lane 1: (E50I60)$_2$ (3321 bp); Lane 2: E100I60E50I60 (4071 bp); Lane 3: E50I60E50I100 (3921 bp); Lane 4: (E50I100)$_2$ (4521 bp); Lanes M: DNA marker 1Kb Plus.DNA agarose.

The digestion with *Xho*I combined with *Xba*I produced two bands, an upper band corresponding to the p7 plasmid and a lower one corresponding to the insert plus 168bp.

Once the constructs were obtained, the following step was to introduce into the expression vector p7, and subsequent transforming of the *E. coli* strain BLR (DE3). Expression was qualitatively assessed by SDS-PAGE. The overexpressing colonies were selected taking into consideration the protein bands pattern. In the following figure (Fig.12) we can observe a SDS-PAGE assay for screening the capacity to produce one of the tetrablock ELRs, in this case E100I60E50I60.
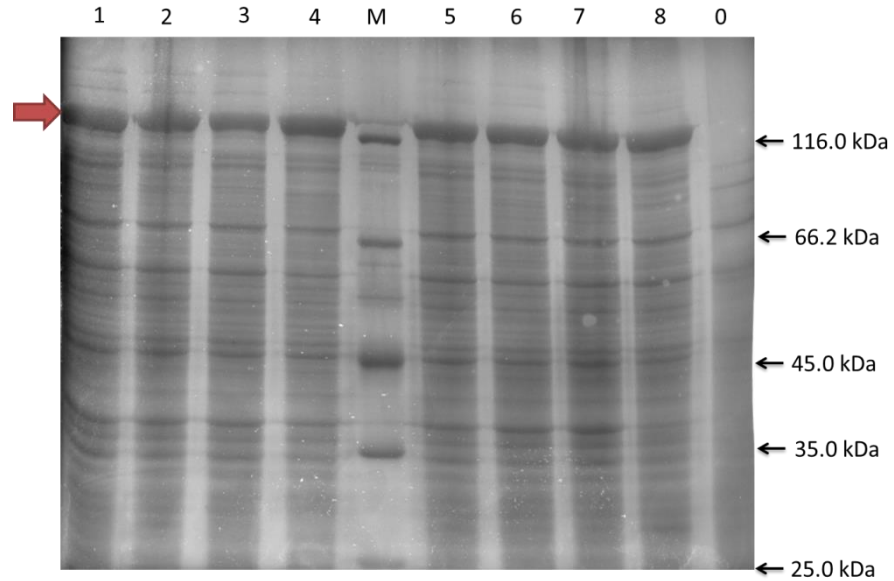
Figure 12 SDS-PAGE of E. coli BLR (DE3) colonies expressing E100I60E50I60 stained with Cooper.

M: Protein Marker (Unstained marker); Lanes 1 to 8: total protein fraction of eight BLR (DE3) ELR E100I60E50I60 producing transformants after overnight induction in TB medium; Lane 0: untransformed BLR as negative control of recombinamer production.

The screening assay showed a slightly variation in recombinamer production between the colonies, nevertheless it is very important to perform first, a small scale experiment of several transformants in order to choose the most suitable for large scale recombinamer expression (**Figure 12**, Lane 4 in this case).

Then, the polymers were produced in large scale and appropriately purified by Inverse Transition Cycling (ITC). The recombinant proteins were purified from the soluble protein fraction as described on 2.2.11.3. As can be seen in the **Figure 13**, a high level of purity is achieved after two IT cycles, despite that three IT cycles were carried out for ensuring that a level of purity greater than 95% is obtained. Following the three IT cycles, the solubilized polymer was dialyzed and lyophilized (see 2.2.11.3).
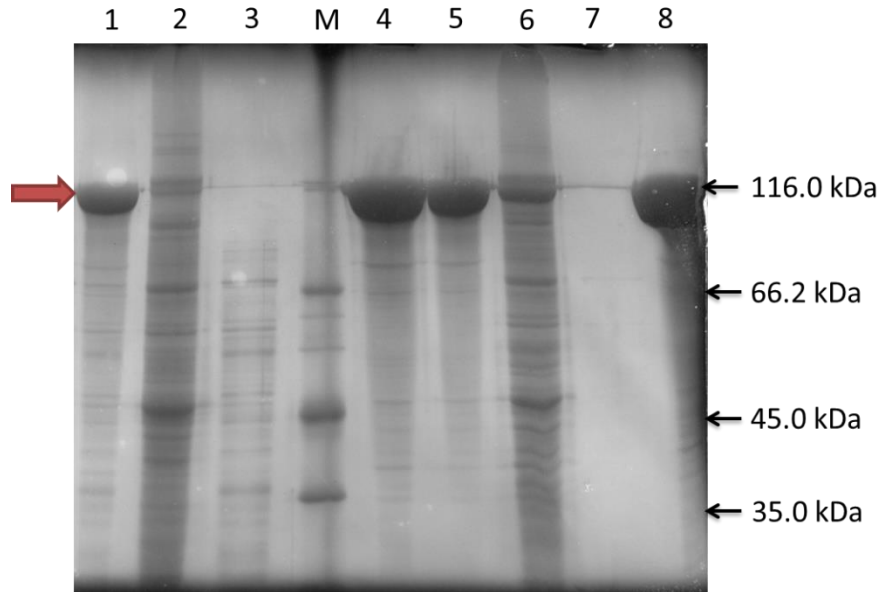
Figure 13 E50I60E50I100 purification analysis by 10% SDS-PAGE stained with Cooper.

Electrophoretic SDS-PAGE image of different stages of the purification procedure of the tetrablock ELR E50I60E50I100. Lane 1: Overnight cold supernatant from the disrupted supernatant; Lane 2: Overnight cold precipitate from the disrupted supernatant; Lane 3: First heating supernatant; Lane 4: First heating precipitate; Lane 5: Overnight cold-dissolved precipitate from first heating; Lane 6: Overnight cold-dissolved supernatant from first heating; Lane 7: Second heating supernatant; Lane 8: Second heating precipitate. M: Marker Unstained.

3.2 MOLECULAR CHARACTERIZATION
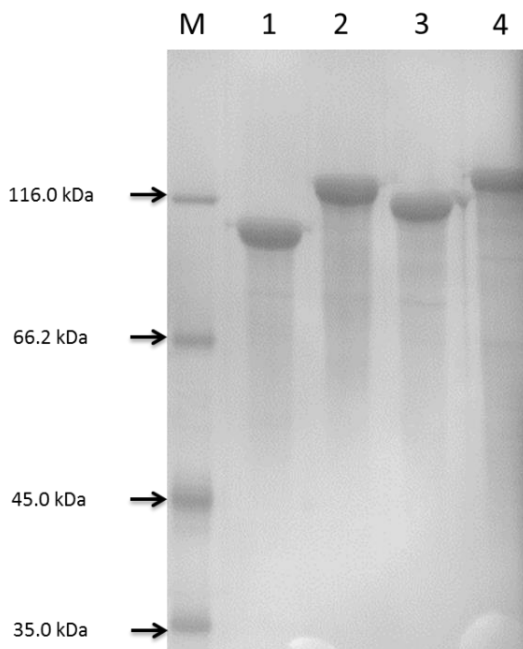
3.2.1 SDS-PAGE

Figure 14 Analysis of the different purified tetrablock-ELRs. 10% SDS-PAGE stained with Cooper.

Lane 1– running pattern of 5µg of the purified recombinamer $(E50I60)_2$. Lane 2– Of the purified E100I60E50I60. Lane 3– Of the purified E50I60E50I100. Lane 4– Of the purified $(E50I100)_2$.

The band although is slightly higher than the theoretical size is within the 20% range, typical of this polymer's, where the ELR run in a polyacrylamide gel. The numbers on the left side of the image correspond to the size in kDa of protein marker reference bands. M: Protein Marker Unstained.

SDS-PAGE analysis lets us verify the purity of the polymer and the correct molecular weight. As we can see, the purity level is over 95%, which demonstrates that the ITC purification method is highly effective and easy to perform.

3.2.2 MALDI-ToF and HPLC analysis

Both, MALDI-ToF and Amino Acid Composition analyses are techniques that confirm the correctness of the expressed recombinant biopolymers. The first method give the information about the protein molecular weight and the theoretical value should be close enough to the one determined by MALDI-ToF and inside the experimental error. The

second, although affected by higher experimental error, gives information about the protein sequence and if there are present any other amino acid not predicted by the DNA sequence.

3.2.2.1   MALDI-ToF Mass Spectrometry Analysis

The MALDI-ToF confirmed the monodisperse character of the purified tetrablock-ELRs. The differences between the theoretical molecular weight and the value experimentally determined are within the experimental error associated with the technique. There are three peaks in each spectrum. The peaks correspond to the whole tetrablock-ELR, and to the double and triple charged species.

The spectrum for the tetrablock $(E50I100)_2$ is missing because it was impossible to perform. The molecular weight of this polymer is 127kDa, and it is on the limit resolution of this technique. Nor has it been possible to find the double charged specie. Nevertheless, as we could see in the electrophoretic SDS-PAGE analysis, the molecular weight of the polymer and its purity correspond to the expected value.
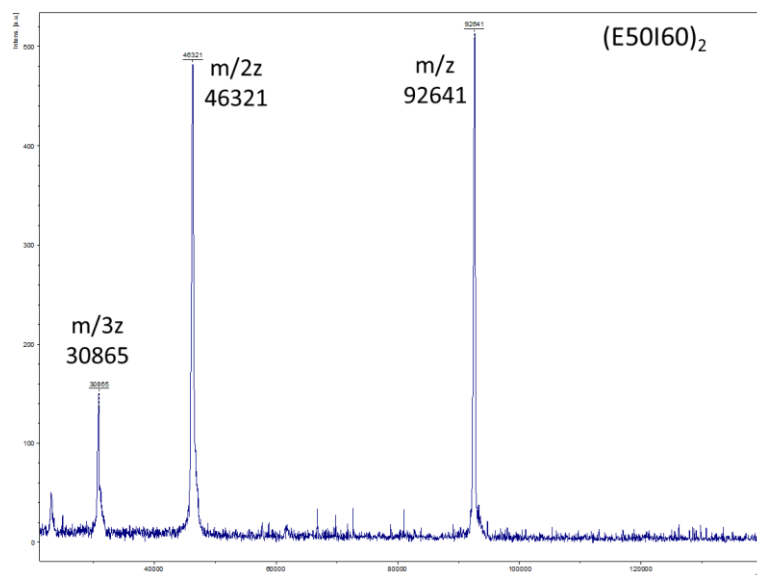

Figure 15 MALDI-ToF mass spectrometry spectrum of the tetrablock (E50I60)$_2$.
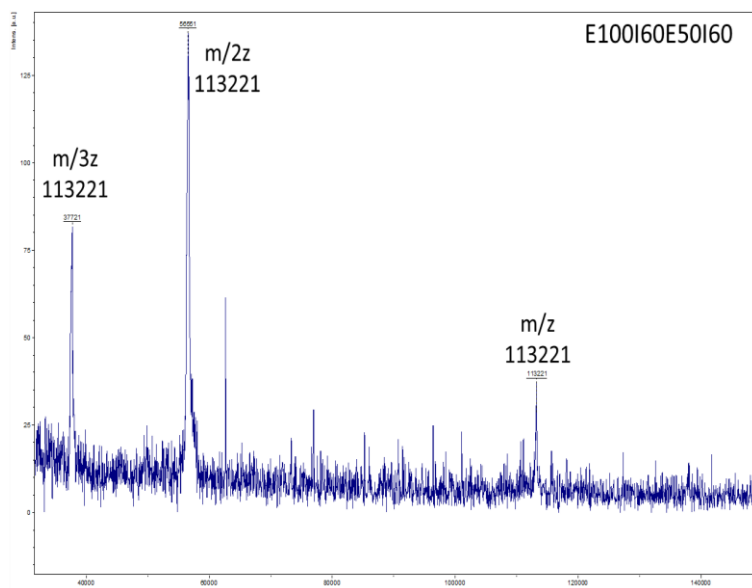
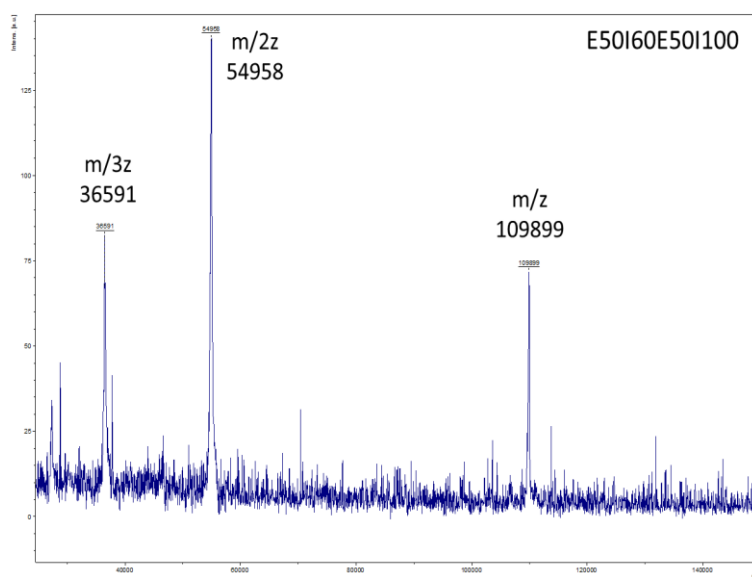**Figure 16 MALDI-ToF mass spectrometry spectrum of the tetrablock E100I60E50I60.**

Figure 17 MALDI-ToF mass spectrometry spectrum of the tetrablock E50I60E50I100.

3.2.2.2   Amino acid Composition Analysis (HPLC)

(E50I60)$_2$		
Amino Acid Residues	*Theoretical Value*	**Experimental Value**

Alanine	*0*	*0.37*
Aspartic Acid	*0*	*0.47*
Glycine	*440*	*432.83*
Glutamic Acid	*21*	*22.01*
Isoleucine	*120*	*119.34*
Leucine	*2*	*1.91*
Lysine	*0*	*0.22*
Methionine	*1*	*0.44*
Proline	*221*	*221.02*
Serine	*1*	*1.09*
Valine	*301*	*304.8*
TOTAL	*1107*	*1104.5*

Table 7 Amino acid composition of the tetrablock ELR (E50I60)2, calculated by HPLC.

E100I60E50I60		
Amino Acid Residues	*Theoretical Value*	*Experimental Value*
Glycine	*640*	*647.23*
Glutamic Acid	*41*	*37.82*
Isoleucine	*120*	*145.94*
Leucine	*2*	*1.96*
Methionine	*1*	*1.68*
Proline	*321*	*322.14*
Serine	*1*	*1.68*
Valine	*481*	*448.76*

TOTAL	*1607*	*1607.21*

Table 8 Amino acid composition of the tetrablock ELR E100I60E50I60, calculated by HPLC.

E50I60E50I100		
Amino Acid Residues	**Theoretical Value**	**Experimental Value**
Glycine	*520*	*524.24*
Glutamic Acid	*21*	*24.74*
Isoleucine	*160*	*156.54*
Leucine	*2*	*2.54*
Methionine	*1*	*334.83*
Proline	*261*	*261.32*
Serine	*1*	*1.33*
Valine	*341*	*334.83*
TOTAL	*1307*	*1307.65*

Table 9 Amino acid composition of the tetrablock ELR E50I60E50I100, calculated by HPLC.

$(E50I100)_2$		
Amino Acid Residues	**Theoretical Value**	**Experimental Value**
Glycine	*600*	*623.52*
Glutamic Acid	*21*	*30.6*
Isoleucine	*200*	*196.77*
Leucine	*2*	*4.31*
Methionine	*1*	*1.78*

Proline	*301*	*310.05*
Serine	*1*	*2.82*
Valine	*381*	*343.38*
TOTAL	*1507*	*1513.23*

Table 10 Aminoacid composition of the tetrablock ELR (E50I100)2, calculated by HPLC.

3.3 Determination of the Inverse Temperature Transition (ITT) by Differential Scanning Calorimetry (DSC) as a function of pH and solvent

Inverse Temperature Transition (ITT) can be determined by Differential Scanning Calorimetry (DSC) a technique described elsewhere[41]. In order to determine the ITT of the tetrablock-ELRs and the solvent and composition dependence three solutions were prepared for each tetrablock (two of those solutions in ultrapure water, at pH<pK$_{Glutamic\ acid}$ and at pH≈7), and the other in PBS buffer (1X).

The solutions for the DSC experiments were prepared at 50 mg/mL in both water and in PBS. The heating program of a typical DSC experiment included an initial isothermal stage (5 min at 0º C for stabilization of the temperature and the state of the polymers), followed by heating at 5º C/min from 0º C to 60º C. The results obtained are summarized in **Figure 18** and **Table 11**.
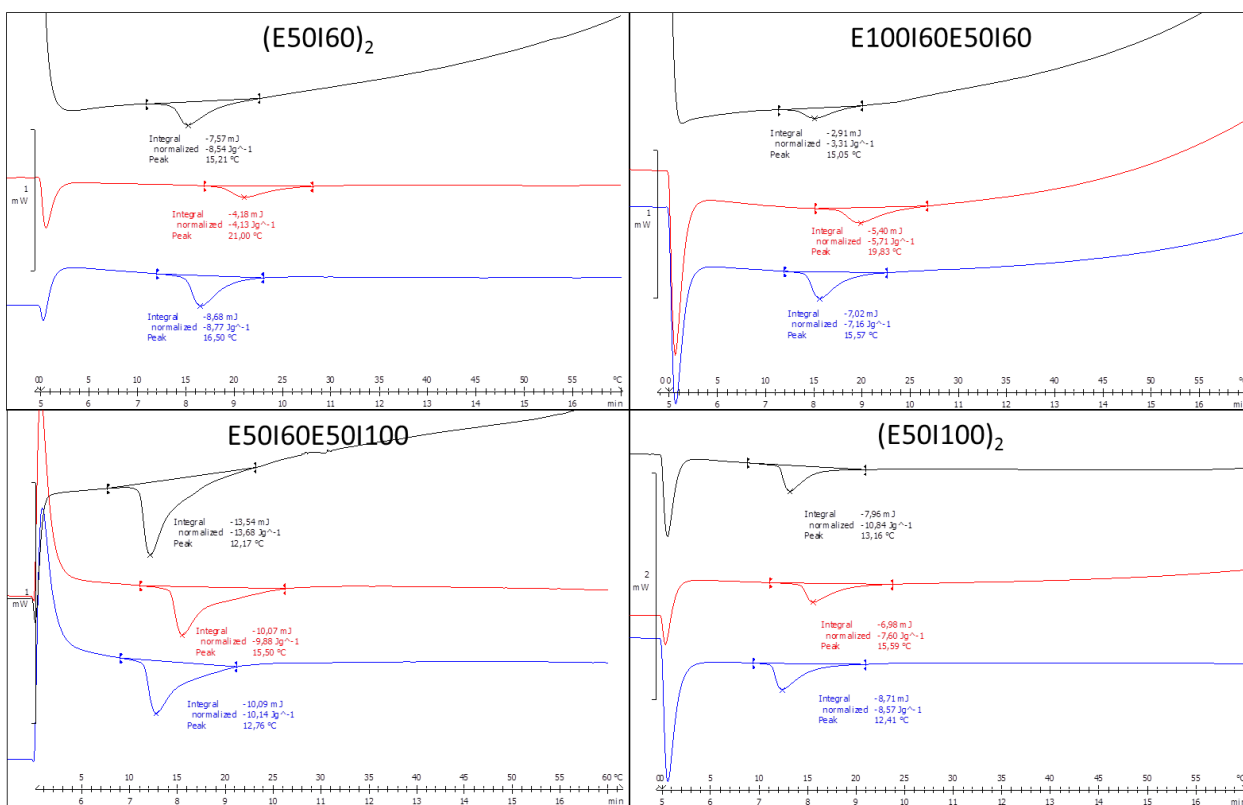
Figure 18 DSC thermograph for a heating cycle (5°C min^{-1}) for the four tetrablock ELRs at 50 mg.mL^{-1}.

	Mw (Da)	Water (pH<pK$_{Glu}$)	Water (pH≈7)	PBS (1X)
(E50I60)$_2$	93157.7	15.2	21	16.5
E100I60E50I60	113931.8	15	19.8	15.6
E50I60E50I100	110098.20	12.2	15.5	12.8
(E50I100)$_2$	127038.7	13.2	15.6	12.4

Table 11 Transition temperatures of the polymers under study in water and PBS.

The ITT is a parameter strongly influenced by the composition of the ELRs but also depends on the molecular mass, concentration, the degree of ionization of any functional side chains, the mean polarity of the polymer, salt concentration and the

presence of other ions and molecules[6].

As expected, in all cases, the ITT is lower in the case of solution in ultrapure water at pH<pK$_{Glu}$ than when at pH≈7. This is due to the fact that at pH below the pKa of carboxylic acid (COOH) of glutamic acid residues in the elastin polypeptide chain, these groups are uncharged (COOH), lowering the interaction with water molecules. This means that there are less water molecules surrounding the protein and therefore a lower temperature or energy is needed in order to break these interactions and promote transition when compared with the solution at pH 7, because in this case, carboxylic groups are deprotonated (COO⁻) and hence the interaction with water molecules is higher than in the other case.

In PBS, there are different ions present in the solution, which lower the ITT independently of the pH that is buffered neutral (pH 7.4), which is very likely to happen in this conditions as described elsewhere.

Comparing the four polymers, the ITT decreases when the ratio hydrophobic block (I): hydrophilic block (E) is increased. But the molecular weight is also a variable of the ITT, and the higher the molecular weight, the lower the transition temperature (T_t) is[46].

$$E50I60E50I100 \approx (E50I100)_2 < E100I60E50I60 \approx (E50I60)_2$$

3.4 ANALYSIS OF THE ABILITY TO ASSEMBLE NANOPARTICLES AND HYDROGELS

3.4.1 Dynamic light scattering

Elastin-like recombinamers composed of block with different hydrophobicities assemble nanostructures[47]. On the basis of the ability of the tetrablock (E50I60)$_2$ to form spherical nanoparticles[2], the nanoparticles formation was studied by DLS. To determine the size of the formed supramolecular structures two series of solutions were prepared (in ultrapure water and in PBS 1X). Thus, the aggregation process has been studied in a solution without any extrinsic factor (Water) and in a solution that mimics the serum salt concentration (PBS).

In order to study the thermal behavior, DLS measurements were carried out using 3 mg/mL solutions of each tetrablock-ELR. The temperature dependence of the intensity of the scattered light when the different solutions were heated is shown in **Figure 19**.
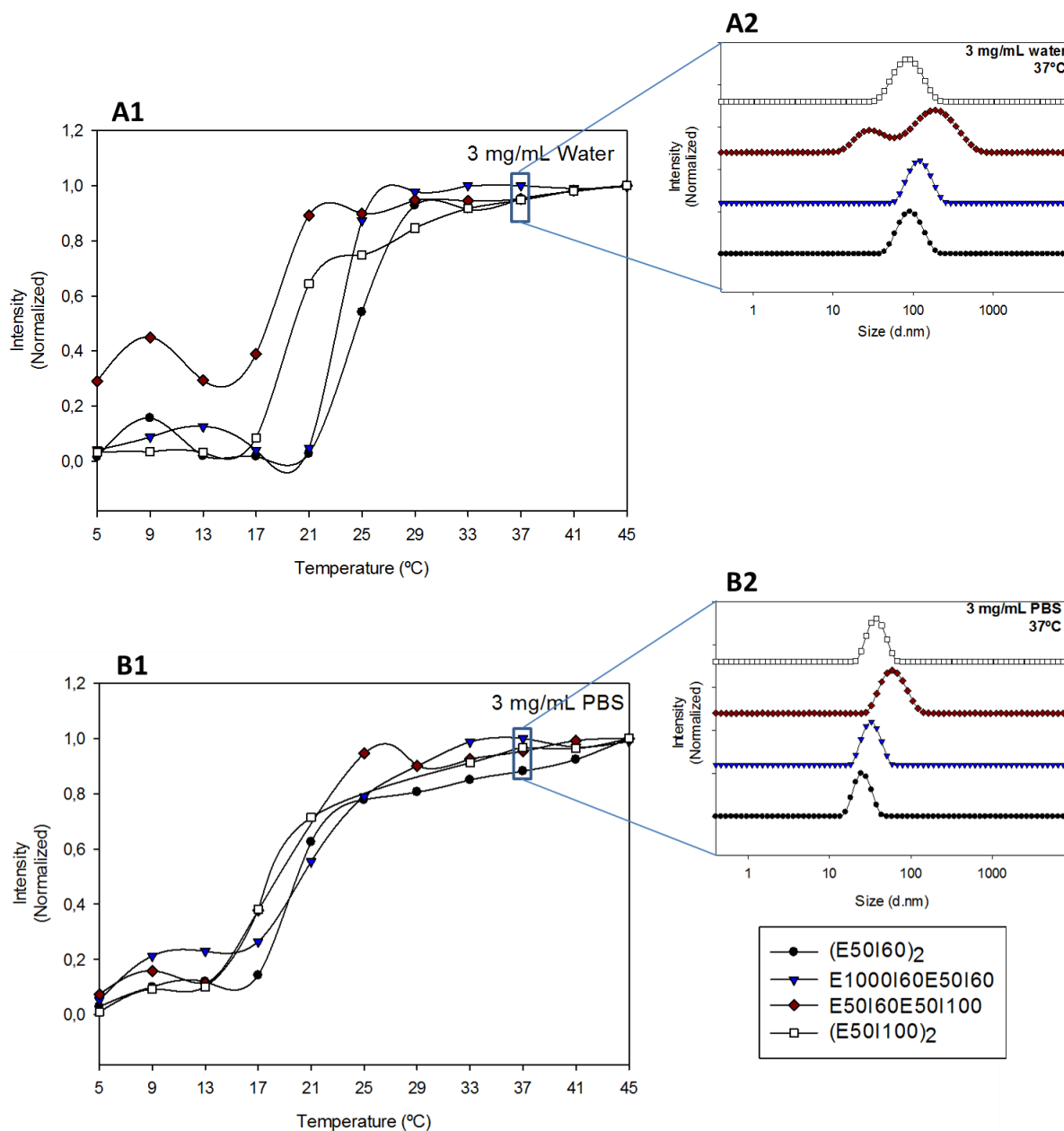

Figure 19 Thermal behavior of the nanostructures formed by the four tetrablock-ELRs.

A: Thermal behavior of the nanostructures formed in **ultrapure water**. A1: Normalized intensity profile of the scattered light as a function of temperature. A2: Normalized size distribution by intensity at 37°C.

B: Thermal behavior of the nanostructures formed in **PBS (1X)**. B1: Normalized intensity profile of the scattered light as

The transition temperature (T_t) or inverse temperature transition (ITT) is taken to be the temperature at which the change in the scattered intensity reaches a value of 50%. T_t differences can be best appreciated in the first plot (**A**), since the effect of buffer ions minimizes T_t differences.

As expected, the T_t decreases when the hydrophilic content increases, as it had been noticed by DSC. But it is also observable the effect of the size proportion between the two hydrophobic blocks of each tetrablock.
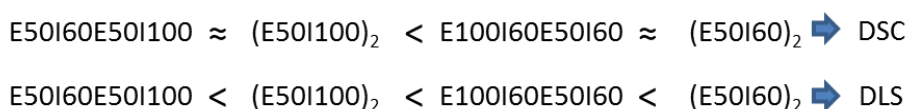
E50I60E50I100 ≈ (E50I100)$_2$ < E100I60E50I60 ≈ (E50I60)$_2$ ➡ DSC

E50I60E50I100 < (E50I100)$_2$ < E100I60E50I60 < (E50I60)$_2$ ➡ DLS

Figure 20 Transition temperatures analyzed by DSC or DLS.

Apparently, this lack of balance between these blocks is involved on the coacervation process, the polymers that present a disproportionate block show a decrease in the T_t, when we are strictly talking about the transition polymer-chains-in solution/polymer-nanoparticles.

In addition, it should be noticed that the salts of the PBS buffer stabilized the nanoparticles, the hydrodynamic diameter decreased and the distributions were more monodisperse, as we can see in the size distributions (**Figure 19, B2**) and in the following table:

	Polydispersity Index (PdI)			
	(E50I60)$_2$	E100I60E50I60	E50I60E50I60100	(E50I100)$_2$
PBS	0,0133	0,031	0,1263	0,0233
Water	0,0983	0,074	0,5427	0,1707

Table 12 Polydispersity Index of the nanoparticles distributions of the tetrablock-ELRs, at a concentration of 3 mg/mL and at temperature of 37ºC.

Moreover, comparing the size distributions based on the scattered intensity (**Figure 19:A2, B2**), it can be seen the influence of the different block combinations in the final formed nanostructures.

Noting that the nanoparticles formed in ultrapure water showed a greater polydispersity, we cannot evaluate the divergences between the diameters of the nanoparticles. We can only suggest that the proportion hydrophobic block (I-block) control the nanoparticle organization. The presence of a disproportion between the two I-blocks (E50I60E50I100) involves an increase in the dispersity of the distribution.

However, the salts present in the buffer stabilize the nanoparticle diameter, and this fact allows us to analyze these divergences. Except for the E50I60E50I100 nanoparticles, that showed greater polydispersity (**Table 12**) and diameter, as a consequence of the presence of an extra I-block at the C-terminal end. The other three tetrablock ELRs self-assembled into highly monodisperse nanoparticles, with different hydrodynamic diameters.
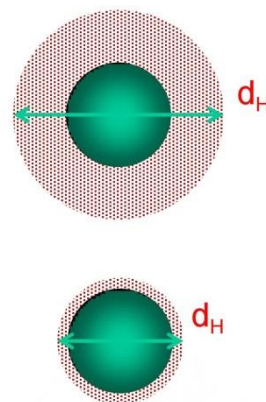
These size divergences cannot be attributed to differences in the sequence, because as we can see on **Table 13**, the diameter divergences can be a consequence of the different molecular weight, not of a different self-assembling pattern.

Figure 21 Ionic strenght effect on the hydrodynamic diameter (D_h)

	(E50I60)$_2$	E100I60E50I60	(E50I100)$_2$	E50I60E50I60100
D_h (PBS)	38.4 nm	49.3 nm	53.4 nm	56.1 nm
Mw	93.2 kDa	113.9 kDa	127.0 kDa	110.1 kDa

Table 13 Nanoparticle hydrodynamic diameters and molecular weights of the four tetrablock-ELRs in PBS.

Once we have verified that the new polymers chains assemble into defined nanostructures at ≈25μM (3mg/mL), the nanoparticles stability at different concentrations were checked. For this, two series of 1, 3, 5, 7 and 10 mg/mL were prepared, in ultrapure
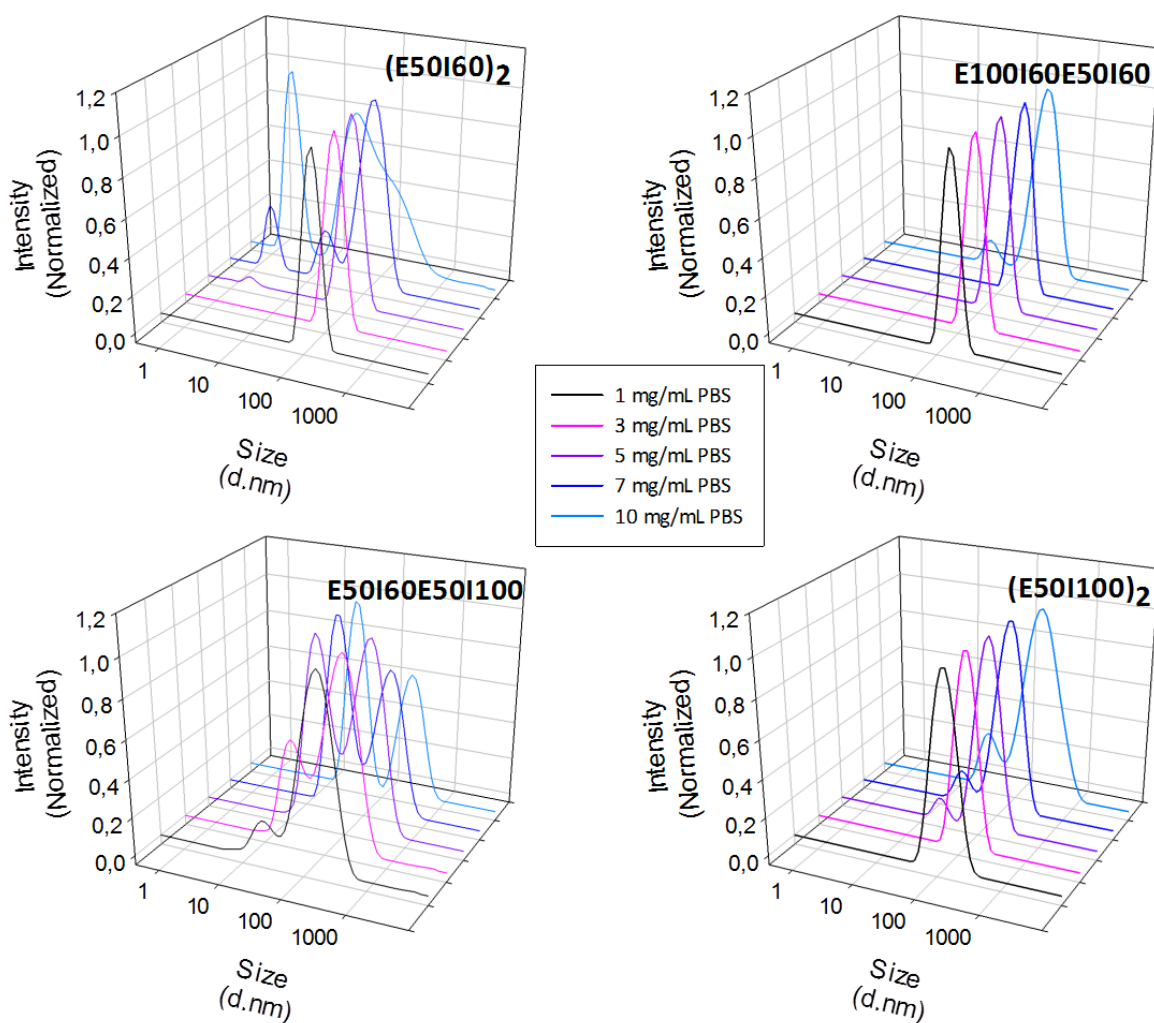
water and in PBS (1X).

Figure 22 Normalized size distributions for different concentrations in ultrapure water of the four tetrablock-ELRs.

If we compare the divergences between the size distributions of the nanostructures formed in water (**Figure 22**) or PBS (**Figure 23**), we may see the effect of the concentration in the nanoparticle stability.

Comparing the distributions in ultrapure water, it is clearly observable that the monodisperse distribution disappeared at concentrations above 3 mg/mL in all the cases except for the recombinamer E100I60E50I60. It can thus be suggested that the increase of hydrophobic content indicates the stabilization of the nanoparticle structure.

Nonetheless, as far as the other three recombinamers, it is a remarkable fact that maintaining the proportion between the hydrophobic blocks (I-blocks), the increase in hydrophobic content enhanced the nanoparticle stability in ultrapure water.
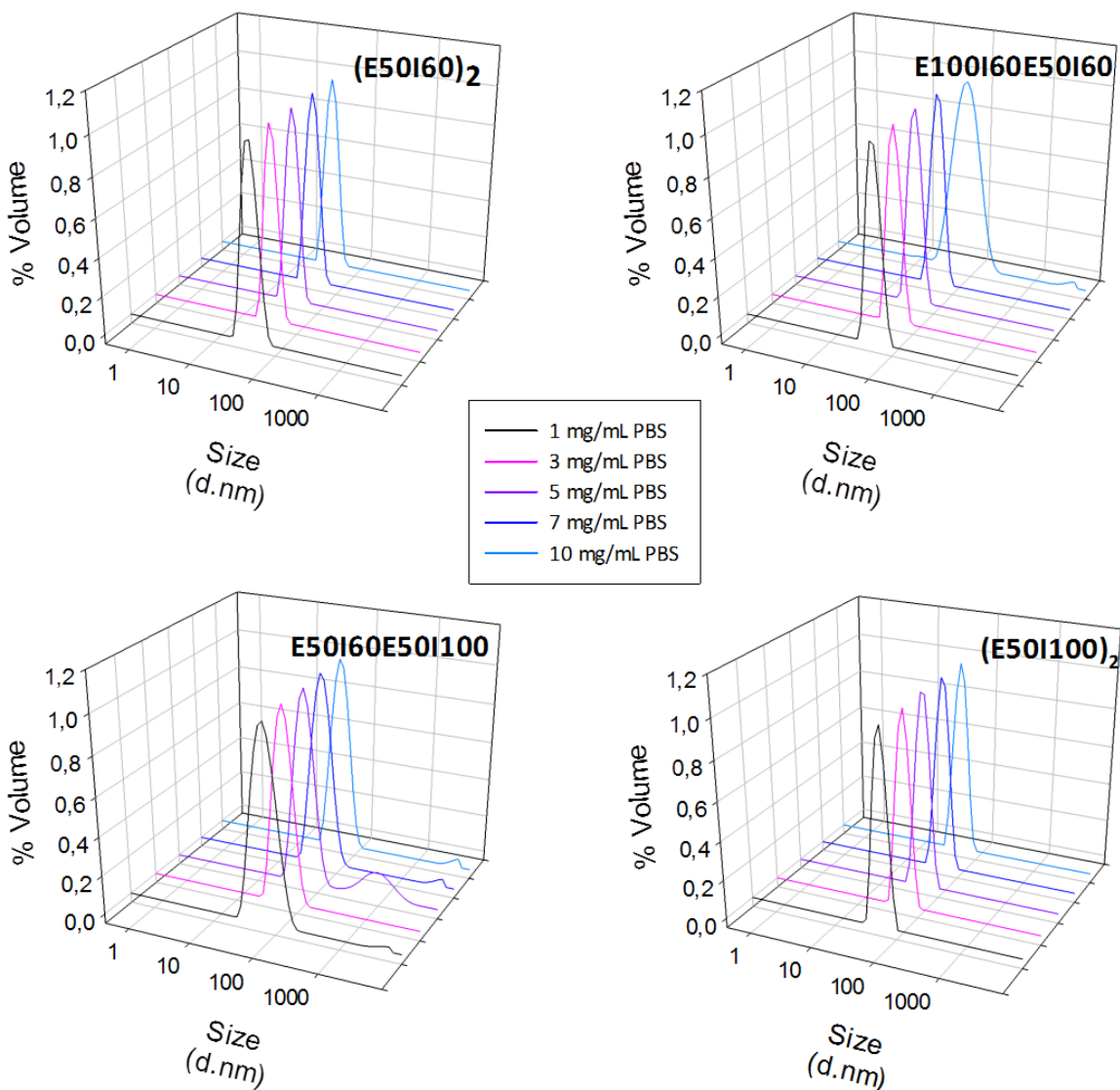

Figure 23 Normalized size distributions for different concentrations in PBS (1X) of the four tetrablock-ELRs.

On the other hand, in PBS the nanoparticles distributions are completely different. As **Figure 23** shows, in all the cases, at all the concentrations the nanoparticles maintained their monodisperse distribution, with the exception of the E50I60E50I100 recombinamer, which was almost not monodisperse.

3.4.1.1   Zeta Potential of the spherical nanoparticles

Z-Potential (mV)				
	(E50I60)$_2$	E100I60E50I60	E50I60E50I60100	(E50I100)$_2$
Water	-31±0.97	-29.3±0.87	-26±1.15	-27.5±0.56
PBS	-8.9±0.83	-7.9±0.74	-8.8±0.87	-9.3±0.97

Table 14 Zeta potential of the ELRs when dissolved in water or PBS at pH≈7 and at 37°C.

Data are presented as the mean ± standard deviation (SD) from three different measurements by performing 10 readings on each.

The four tetrablock nanoparticles when dissolved in ultrapure water at neutral pH rendered negative surface charges because the presence of glutamic acids. Generally a Z-potential of +/-30mV is considered a suitable threshold value for colloidal stability[48]. As we can see in **Table14**, in all four cases the potentials are around this value. That confirms that the nanoparticles are electrostatically stable.

On the other hand, the presence of salts, when the Z-potential determinations were carried out in PBS, drastically increased the resulting zeta potential value. The ionic interactions between the buffer salts and the nanoparticles masked the superficial charge of the nanoparticles.

3.4.2 Cryo-Transmission Electron Microscopy (Cryo-TEM)

The spherical nanoparticles observed by DLS were also verified by cryo-TEM. Buffered solutions of the four recombinamers were dissolved (25 μM in PBS) at 4°C O/N, after that the solutions were equilibrated at 37°C during at least 1hour. The results are shown in the **Figures 24** and **25**.
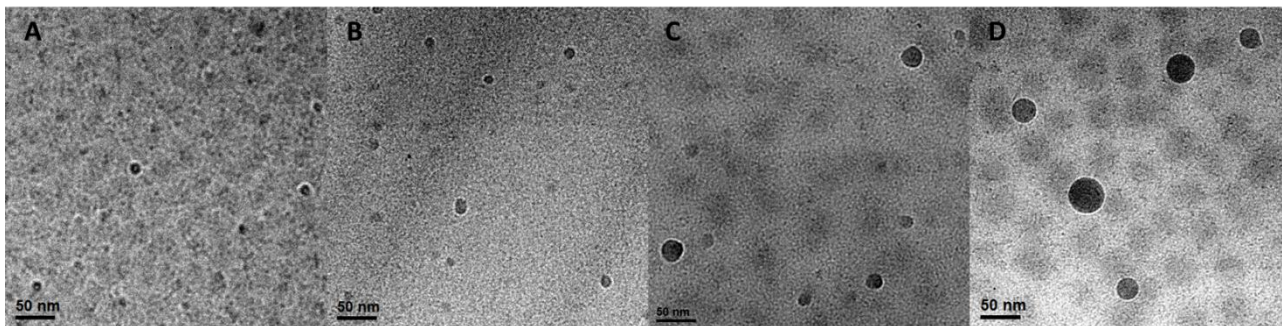
Figure 24 Cryo-TEM images of the nanoparticles formed by the different tetrablock-ELRs at 37°C in PBS.

A: (E50I60)$_2$; B: E100I60E50I60; C: E50I60E50I100; D: (E50I100)$_2$

Spherical nanoparticles were observed by cryo-TEM in all the cases. The nanoparticle diameters noticed are shown in the following table:

	(E50I60)$_2$	E100I60E50I60	E50I60E50I60100	(E50I100)$_2$
D_h (PBS) [DLS]	38.4	49.3	56.1	53.4
Diameter [Cryo-TEM]	14.7±1.8	18±2.7	22.8±5.4	35.2±7.7
Mw	93.2 kDa	113.9 kDa	110.1 kDa	127.0 kDa

Table 15 Comparative table of the different diameters measured by DLS and Cryo-TEM.

The differences observed between the nanoparticles diameters measured by DLS or by cryo-TEM are mainly due to the fact that the measurements done by DLS consider the hydrodynamic diameter (the nanoparticle and its hydratation sphere), and this is the reason why the nanoparticles are smaller.
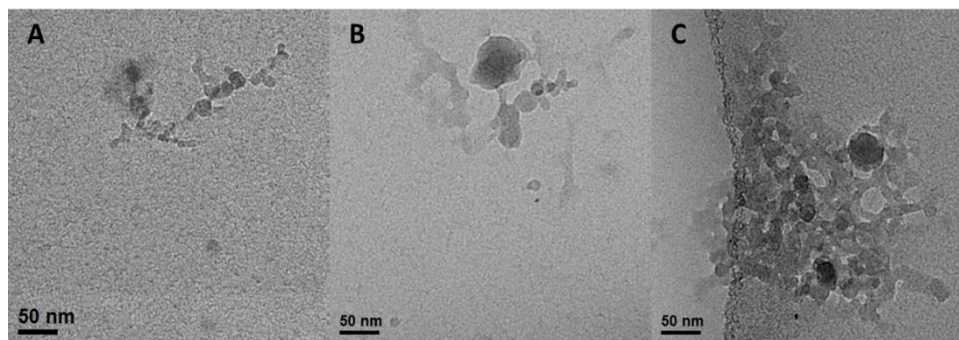
Figure 25 Cryo-TEM images of the protogels formed by the (E50I100)$_2$ recombinamer at 37°C in PBS.

It is also worth noting that when the images were taken other nanostructures more complex were found. This nanostructures were found only in the samples prepared with the recombinamer (E50I100)$_2$. As we can see in **Figure 25**, these nanostructures are based on aggregations of nanoparticles. These protogels will result in the formation of the final physical hydrogel. Similar nanogels have been described previously[49] but in this case they were based on a chemical approach.

3.4.3 Rheological characterization

Amphiphilic ELRs are a promising class of biomaterials with applications including drug delivery and tissue engineering. The demonstrated ability[2] of the ELRs based on amphiphilic-tetrablocks to form hydrogel makes these kind of recombinamers an attractive option to design biomimetic scaffolds that can act as the extracellular matrix (ECM).

These hydrogels would have a mainly importance in the biomedical field. Due to the Elastin-like thermoresponsive nature, these hydrogels could be used as injectable systems, which would imply several advantages including patient comfort and cost reduction.

Rheological measurements were performed to evaluate the relationships between molecular structure and viscoelastic behavior of the tetrablock-ELRs. Different solutions at 250, 275 and 300 mg/mL of each tetrablock ELR were prepared in ultrapure water and PBS (1X). The most representative results (at 275mg/mL) are shown.

The thermogelling properties of the eigth solutions were evaluated as a function of temperature using a controlled stress rheometer at a constant strain of 0.3% and a frequency of 1 Hz (**Figure 27 (Water)** and **28 (PBS)**). A strain of 0.3% was selected because this frecuency is located on the linear viscoelastic (LVE) region of the materials (**Figure 26**). The determination of the LVE region is important because it allows for the determination of the range of percent strains that are acceptable for use in later tests. If a percent strain is utilized that exceeds the percent strain in the LVE region the mechanical structure of the sample will be compromised and thus the data collected may be inaccurate.
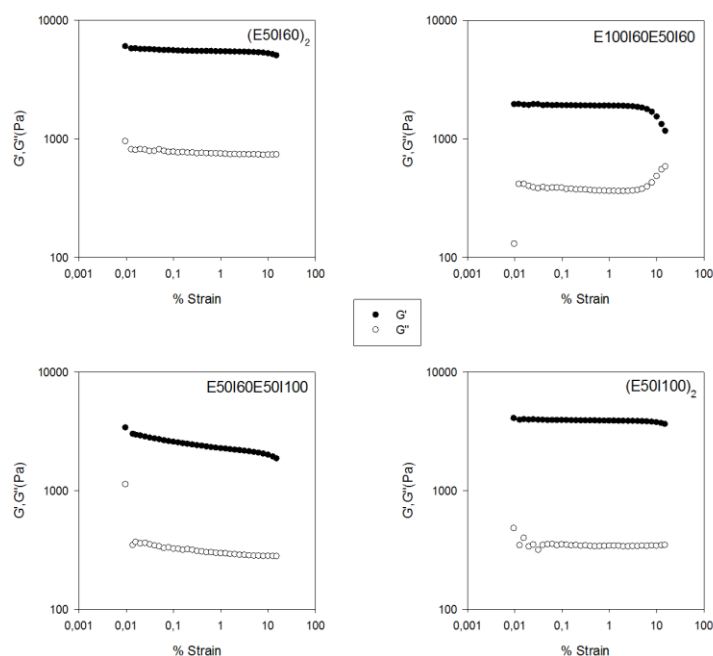

Figure 26 Strain dependance of the storage and loss modulus at 37°C and 1Hz.

Determined a strain value, the thermal behavior was analyzed. For this purpose, two temperature ramps were performed (heating and cooling ramp) from 5 to 40°C (and from 40 to 5°C), and time sweeps at 37°C.
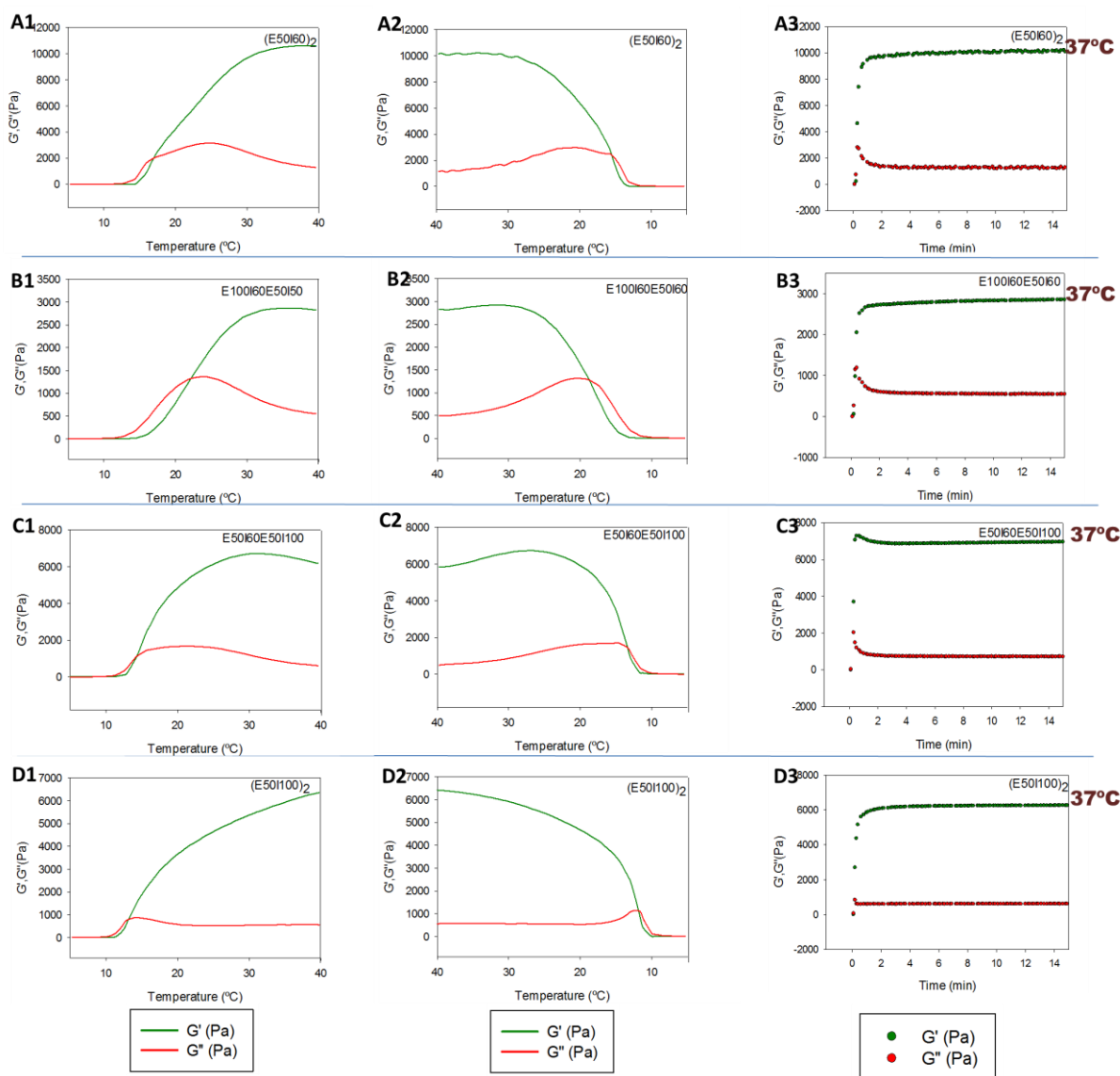
3.4.3.1 Hydrogels formed in Ultrapure Water

First, the temperature ramps were carried out. The plots of the thermogelling properties as a function of the temperature revealed a gelation temperature $(G'=G'')$[50,51] and the maximus storage moduli of the four recombinamer solutions in water (**Table 16**).

After that, time sweeps at 37°C were performed with the same solutions to accurately report the equilibrium moduli (**Table 16**) at physiological temperature and the gelation time. The gelation process was an instantaneous process. As we can see in the

time sweep plots, less than 1 minute was required to the hydrogels conformation.

	(E50I60)$_2$	E100I60E50I60	E50I60E50I100	(E50I100)$_2$
Gelation T(ºC)	17	22	14.4	13.2
Maximus G'	10620 Pa (40ºC)	2868 Pa (35ºC)	7273Pa (30ºC)	6360 Pa (40ºC)
Linear equilibrium modulus (37ºC)	10100 Pa	2830 Pa	6900 Pa	6250 Pa

Table 16 Gelification temperatures and storage moduli when the 275 mg/mL hydrogels were formed in ultrapure water.

As we can see in **Table 16,** practically there are no difference between the maximus storage moduli and the linear storage moduli. Analyzing the four time sweeps, we can observe that in all the cases the storage moduli reached their greatest value at 37ºC, and after that remained stable.

It is also worth noting that the gelation process is a reversible process. It was clearly demonstrated because during the rheological analysis the recombinamers solutions experienced three transitions; first it was carried out the heating ramp (5→40ºC), then cooling ramp (40→5ºC), and finally the time sweep (5→37 and 15' at 37ºC) (in **Figure 27** numbers **1, 2, 3**).
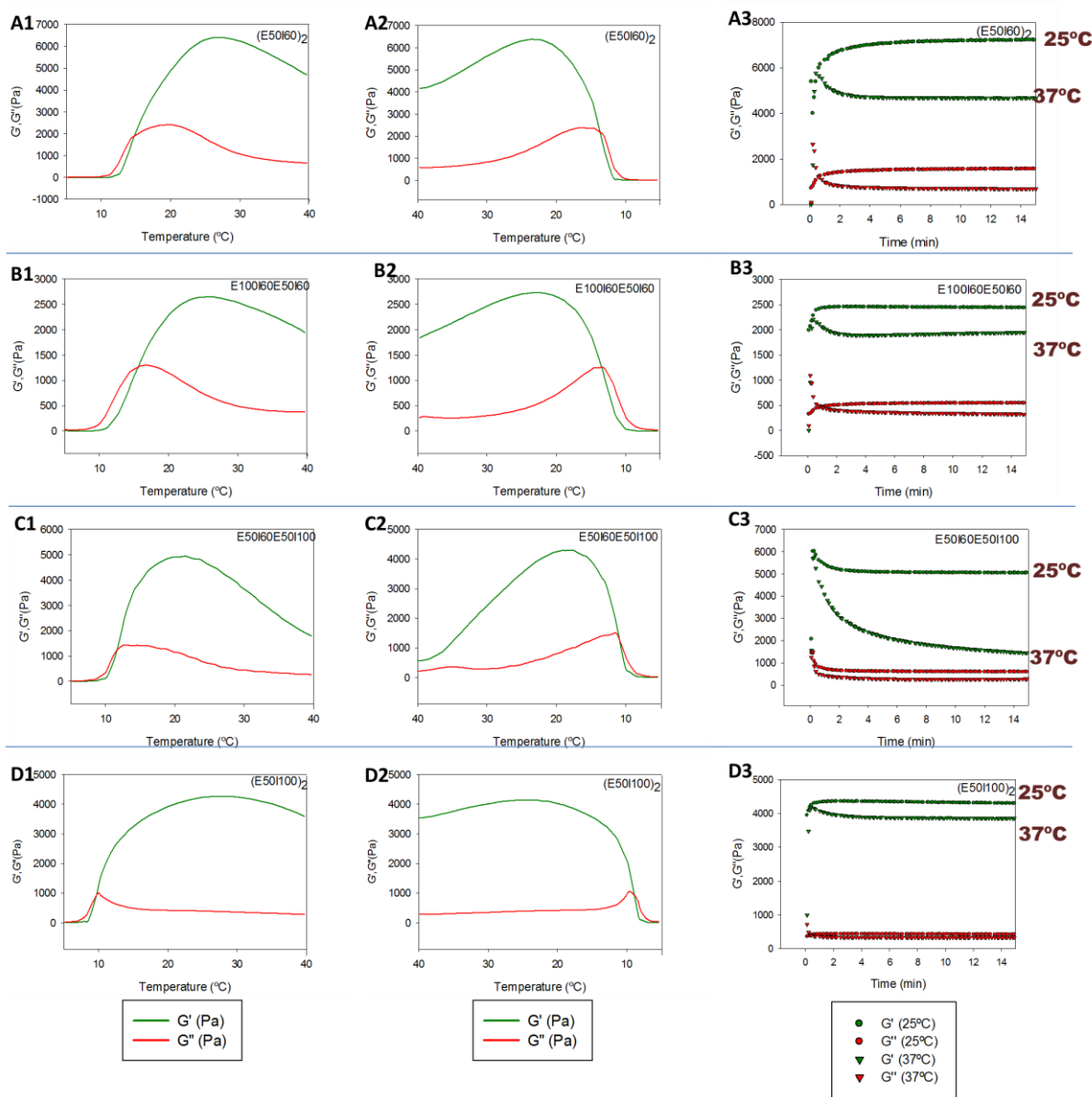
Figure 28 Evolution of loss and storage modulus of 275 mg/mL PBS (1X) as a function of temperature and time. The letters correspond to the four tetrablock-ELRs: A-(E50I60)₂; B- E100I6050I60; C- E50I60E50I100; D-(E50I100)₂. And the numbers correspond to the experimental process: 1-Heating ramp (5-40°C); 2-Cooling ramp (40-5°C); 3-Time sweeps (25 and 37°C).

The thermal behavior of the different tetrablock-ELRs solutions in PBS is shown in **Figure 28**. At it happened in ultrapure water solutions the recombinamers showed in PBS; an instantaneous and reversible gelification process. But unexpectedly a new thermogelling behavior appeared.

In this case, the storage moduli behavior changes completely. The maximum

58

storage moduli were considerably decreased, and this value was reached around the 20-25ºC, depending on the recombinamer. After that the modulus began to be reduced if the temperature was increased, if not (as we can see in the time sweeps A3, B3, C3 and D3 of the **Figure 28**) the modulus maintained over the time.

This behavior suggests the presence of two different states of organization. The interaction of the ions presents in the buffer with the hydrophobic blocks of the tetrablock-ELRs (VGIPG) conditions the self-organization of the hydrogel (maximum modulus values decrease with respect water). This hydrogel organization was stable over time, but when we gave energy to the system (temperature was increased) this state began to self-reorganize into softer hydrogel forms.

It is particularly noteworthy the E50I60E50I100 and the (E50I100)$_2$ behavior. In the first case, the abrupt changes of its modulus stood out from the rest. A possible explanation for this might be that the disproportion between the hydrophobic blocks determines the thermal stability of the new chains organization. In the second one [(E50I100)$_2$], it should be noted that a proportional increase of the hydrophobic content suggests the formation of a thermal-stable hydrogel. In this recombinamer the modulus fall was the smallest (as we can see on **Table 17**). This behavior is consistent with the images obtained by cryo-TEM. This tetrablock ELR show a tendency to form hydrogels and these are more thermal-stable.

	(E50I60)$_2$	E100I60E50I60	E50I60E50I100	(E50I100)$_2$
Gelation T(ºC)	15.7 (17)	15.6 (22)	11.4 (14.4)	9.8 (13.2)
Maximus G'	6412 Pa (27ºC)	2650 Pa (26ºC)	4945 Pa (21ºC)	4268 Pa (27ºC)
Linear equilibrium modulus (37ºC)	4670 Pa	1940 Pa	1500 Pa	3850 Pa

Table 17 Gelification temperatures and storage moduli when the 275 mg/mL hydrogels were formed in PBS (1X).

Lastly, looking at the results obtained, we can assert that the mechanical strength of the tetrablock based hydrogels is tunable. Changes on the ratio hydrophobic blocks (I-

blocks): hydrophilic blocks (E-blocks) have a negative effect on the mechanical strength. As it could be noticed, comparing the rheological behavior of the new constructions with the $(E50I60)_2$ behavior, the storage moduli (G') significantly decrease in the cases of the 'asymmetric' tetrablock-ELRs (E100I60E50I60 and E50I60E50I100).

What is surprising is that the mechanical properties were not improved in the case of the $(E50I100)_2$ recombinamer. This ELR was intended to have greater moduli; therefore it contains two hydrophobic blocks longer than $(E50I60)_2$. Nor was it improved, only it was improved the dynamic behavior in PBS. After the gelation temperature the hydrogel state formed showed the greater thermal stability.

4   CONCLUSION

The intrinsic ability of the ELRs to self-assemble into complex supramolecular nanostructures makes these materials a highly attractive alternative to biomedical applications, in terms of biocompatibility, cost effectiveness and extremely specific functionalities.

In this Master thesis, we present a study on the effect of the size proportion of the individual blocks on the ability of tetrablock-Elastin-like-Recombinamers to self-assemble into nanoparticles and hydrogels. For this reason, four biopolymers were recombinantly produced and physico-chemically characterized.

Results presented here demonstrate that the size proportion between the hydrophobic and hydrophilic blocks is a factor that predetermines the supramolecular organization of the nanoparticles and the hydrogels.

The 'asymmetry' between the diblocks that forms a tetrablock seems to have hardly any effect on the self-organization of the spherical nanoparticles. The divergences observed on the nanoparticle diameter were not significant; these can be a consequence of the differences in the molecular weight of the individual chains.

On the other hand, this asymmetry seems to have a profound effect on the viscoelastic properties of the hydrogels. The proportion between the hydrophobic and the hydrophilic blocks directly influences the storage modulus. When the proportion hydrophobic block **:** hydrophilic block ≈ 1 is broken the storage modulus value decreases considerably. But even though this fall, when both hydrophobic blocks were increased [(E50I100)$_2$] the hydrogel formed show an improved thermodynamic behavior, and an unusual feature; the presence of physical nanogels at low concentrations.

In conclusion, we have demonstrated that not only the disposition of the blocks, but also the proportionality between the hydrophobic and hydrophilic parts have influence over the thermogelling mechanical properties of the physical hydrogels. Moreover, these new biomaterials have future applications as nanocarriers for drug delivery and as injectable hydrogels for tissue regeneration.

REFERENCES

(1)   Laurencin, C. T.; Nair, L. S. *Nanotechnology and tissue engineering: the scaffold*; CRC Press, 2008.

(2)   Martin, L.; Javier Arias, F.; Alonso, M.; Garcia-Arevalo, C.; Rodriguez-Cabello, J. C. *Soft Matter* **2010**, *6*, 1121.

(3)   Whitesides, G. M. *Small* **2005**, *1*, 172.

(4)   Sanchez, F.; Sobolev, K. *Construction and Building Materials* **2010**, *24*, 2060.

(5)   Hu, X.; Cebe, P.; Weiss, A. S.; Omenetto, F.; Kaplan, D. L. *Materials Today* **2012**, *15*, 208.

(6)   Rodríguez-Cabello, J. C.; Martín, L.; Alonso, M.; Arias, F. J.; Testera, A. M. *Polymer* **2009**, *50*, 5159.

(7)   Girotti, A.; Fernandez-Colino, A.; Lopez, I. M.; Rodriguez-Cabello, J. C.; Arias, F. J. *Biotechnol. J.* **2011**, *6*, 1174.

(8)   Rodríguez-Cabello, J.; Girotti, A.; Ribeiro, A.; Arias, F. In *Nanotechnology in Regenerative Medicine*; Navarro, M., Planell, J. A., Eds.; Humana Press: 2012; Vol. 811, p 319.

(9)   MacEwan, S. R.; Chilkoti, A. *Peptide Science* **2010**, *94*, 60.

(10)   Vrhovski, B.; Weiss, A. S. *European Journal of Biochemistry* **1998**, *258*, 1.

(11)   Uitto, J. *Journal of Investigative Dermatology* **1979**, *72*, 1.

(12)   Li, B.; Alonso, D. O. V.; Bennion, B. J.; Daggett, V. *Journal of the American Chemical Society* **2001**, *123*, 11991.

(13)   Li, B.; Alonso, D. O. V.; Daggett, V. *Journal of Molecular Biology* **2001**, *305*, 581.

(14)   Miao, M.; Bellingham, C. M.; Stahl, R. J.; Sitarz, E. E.; Lane, C. J.; Keeley, F. W. *Journal of Biological Chemistry* **2003**, *278*, 48553.

(15)   Simnick, A. J.; Lim, D. W.; Chow, D.; Chilkoti, A. *Journal of Macromolecular Science, Part C: Polymer Reviews* **2007**, *47*, 121.

(16)   Rodríguez-Cabello, J. C.; Reguera, J.; Girotti, A.; Arias, F. J.; Alonso, M. *Advances in Polymer Science* **2006**, *200*, 119.

(17)   Urry, D. W. *What sustains life? Consilient mechanisms for protein-based machines and materials*; Springer-Verlag: New York, 2006.

(18)   McPherson, D. T.; Xu, J.; Urry, D. W. *Protein expression and purification* **1996**, *7*, 51.

(19)   Reguera, J.; Alonso, M.; Testera, A. M.; López, I. M.; Martín, S.; Rodríguez-Cabello, J. C. *Carbohydrate Polymers* **2004**, *57*, 293.

(20)   Mithieux, S. M.; Weiss, A. S. *Advances in protein chemistry* **2005**, *70*, 437.

(21)   Debelle, L.; Tamburro, A. *The international journal of biochemistry & cell biology* **1999**, *31*, 261.

(22)   Rodriguez-Cabello, J. C.; Gonzalez de Torre, I.; Pinedo, G. In *Smart Materials for Drug Delivery: Volume 2*; The Royal Society of Chemistry: 2013; Vol. 2, p 180.

(23)   Reguera, J.; Alonso, M.; Testera, A. M.; Lopez, I. M.; Martin, S.; Rodriguez-Cabello, J. C. *Carbohydrate Polymers* **2004**, *57*, 293.

(24)   Li, B.; Daggett, V. *Biopolymers* **2003**, *68*, 121.

(25)   Rodríguez-Cabello, J. C. *Biomaterials: From Molecules to Engineered Tissues* **2004**, *553*, 45.

(26)   Rodríguez-Cabello, J. C.; Alonso, M.; Guiscardo, L.; Reboto, V.; Girotti, A. *Advanced Materials* **2002**, *14*, 1151.

(27)   Urry, D. W. *Trends Biotechnol* **1999**, *17*, 249.

(28)   Urry, D. W.; Peng, S. Q.; Hayes, L. C.; McPherson, D.; Xu, J.; Woods, T. C.; Gowda, D. C.; Pattanaik, A. *Biotechnol Bioeng* **1998**, *58*, 175.

(29)   Findenegg, G. H. *Berichte der Bunsengesellschaft für physikalische Chemie* **1986**, *90*, 1241.

(30)   Nagarajan, R.; Ganesh, K. *Macromolecules* **1989**, *22*, 4312.

(31)   Jones, R. A. *Soft condensed matter*; Oxford University Press, 2002; Vol. 6.

(32)   Castelletto, V.; Parras, P.; Hamley, I.; Bäverbäck, P.; Pedersen, J. S.; Panine, P. *Langmuir* **2007**, *23*, 6896.

(33)   Discher, B. M.; Won, Y. Y.; Ege, D. S.; Lee, J. C. M.; Bates, F. S.; Discher, D. E.; Hammer, D. A. *Science* **1999**, *284*, 1143.

(34)   Jain, S.; Bates, F. S. *Science* **2003**, *300*, 460.

(35)   Cui, H.; Chen, Z.; Zhong, S.; Wooley, K. L.; Pochan, D. J. *Science* **2007**, *317*, 647.

(36)   Rodríguez-Cabello, J. C.; Alonso, M.; Diez, M. I.; Caballero, M. I.; Herguedas, M. M. *Macromolecular Chemistry and Physics* **1999**, *200*, 1831.

(37)   *Elastin-like systems for tissue engineering*

Woodhead Publishing Limited (Ed. by R. L. Reis)

ed.; Rodríguez-CabelloJ.C. , A. R., Reguera J. , GirottiA., TesteraA. M. , Ed., 2008.

(38)   Rodríguez-Cabello, J. C.; Reguera, J.; Girotti, A.; Alonso, M.; Testera, A. M. *Progress in Polymer Science* **2005**, *30*, 1119.

(39)   Martín, L.; Castro, E.; Ribeiro, A.; Alonso, M.; Rodríguez-Cabello, J. C. *Biomacromolecules* **2012**, *13*, 293.

(40)   Chung, C.; Niemela, S. L.; Miller, R. H. *Proceedings of the National Academy of Sciences* **1989**, *86*, 2172.

(41)   Ribeiro, A.; Arias, F. J.; Reguera, J.; Alonso, M.; Rodriguez-Cabello, J. C. *Biophys J* **2009**, *97*, 312.

(42)   Laemmli, U. K. *nature* **1970**, *227*, 680.

(43)   Rodríguez-Cabello, J. C.; Alonso, M.; Perez, T.; Herguedas, M. M. *Biopolymers* **2000**, *54*, 282.

(44)   Lee, C.; Levin, A.; Branton, D. *Analytical biochemistry* **1987**, *166*, 308.

(45)   Park, C.; Yoon, J.; Thomas, E. L. *Polymer* **2003**, *44*, 6725.

(46)   Meyer, D. E.; Chilkoti, A. *Biomacromolecules* **2004**, *5*, 846.

(47)   Rodriguez-Cabello, J. C.; Girotti, A.; Ribeiro, A.; Arias, F. J. In *Nanotechnology in Regenerative Medicine*; Navarro, M., Planell, J. A., Eds.; Humana Press: 2012; Vol. 811, p 319.

(48)   Larsson, M.; Hill, A.; Duffy, J.; AB, M. I. N. *Ann. Trans. Nordic Rheol. Soc* **2012**, *20*, 209.

(49)   González de Torre, I.; Quintanilla, L.; Pinedo-Martín, G.; Alonso, M.; Rodríguez-Cabello, J. C. *ACS applied materials & interfaces* **2014**, *6*, 14509.

(50)   Tung, C.-Y. M.; Dynes, P. J. *J. Appl. Polym. Sci.* **1982**, *27*, 569.

(51)   Winter, H. H.; Chambon, F. *J. Rheol.* **1986**, *30*, 367.